CHALMERS
UNIVERSITY OF TECHNOLOGY

Harmonic distortion analysis involving submarine cables for offshore wind power plants

A thesis conducted at Hitachi Energy Sweden AB

Master's thesis in Electric Power Engineering

Gabriel Hassellöf

DEPARTMENT OF ELECTRICAL ENGINEERING

CHALMERS UNIVERSITY OF TECHNOLOGY
Gothenburg, Sweden 2026
chalmers.se

MASTER'S THESIS 2026

A master's thesis investigating the correlation between grid strength, cable length and injected voltage harmonics in offshore wind power systems through analysis of voltage harmonics and harmonic impedance at the point of common coupling.

Gabriel Hassellöf

CHALMERS
UNIVERSITY OF TECHNOLOGY

Department of Electrical Engineering
Division of Electric Power Engineering
CHALMERS UNIVERSITY OF TECHNOLOGY
Gothenburg, Sweden 2026

A master's thesis investigating the correlation between grid strength, cable length and injected voltage harmonics in offshore wind power systems through analysis of voltage harmonics and harmonic impedance at the point of common coupling.
Gabriel Hassellöf

Supervisor: Emil Lindström, Hitachi Energy Sweden AB
Examiner: Professor Massimo Bongiorno, Department of Electrical Engineering

Master's Thesis 2026
Department of Electrical Engineering
Division of Electric Power Engineering
Chalmers University of Technology
SE-412 96 Gothenburg
Telephone +46 31 772 1000

Cover: Rampion Offshore Wind Farm off the coast of Brighton, UK, with wind turbines and an offshore substation. Photo: Gabriel Hassellöf, 2024.

Gothenburg, Sweden 2026

A master's thesis investigating the correlation between grid strength, cable length and injected voltage harmonics in offshore wind power systems through analysis of voltage harmonics and harmonic impedance at the point of common coupling.

Gabriel Hassellöf
Department of Electrical Engineering
Chalmers University of Technology

Abstract

With offshore wind power plants (OWPPs) getting larger and more common, the connection requirements at the point of common coupling (PCC) become more important. OWPPs often use converters that produce harmonics, and reactive components such as long high voltage AC (HVAC) submarine export cables further influence the harmonic content seen at the PCC.

This thesis looks at voltage harmonics up to the 63rd order at the PCC between an OWPP and the main grid. An aggregated type IV OWPP with grid-following converters was modeled in PSCAD, and the harmonic content was analyzed in MATLAB using a fast Fourier transform (FFT). The simulated cases varied three factors: grid strength (a stronger and a weaker grid, relative to each other), HVAC export cable length (50 km and 100 km), and the order of voltage harmonic injected from the main grid (5th and 9th). Results are presented in the voltage and harmonic impedance domains. The impedance analysis focuses on the resistive component, since the reactive component remained inductive for all simulated cases.

Grid strength was the dominant factor in the post-energization transient. Weaker grids produced a total harmonic distortion (THD) of 31-41 %, which is 2-4 times higher than the 9-19 % seen for stronger grids in the same cases. A sensitivity check on later FFT windows showed that both grid configurations settle at a similar low THD around 2 %. The 2-4 times ratio is therefore specific to the post-energization transient, rather than the steady-state.

The aggregated model is appropriate for studying the interaction between grid strength, cable parameters, and injected harmonics. Within the factors studied, grid strength had a much larger effect on THD than cable length, which means that grid reinforcement is more impactful than cable routing for limiting harmonic distortion at the PCC. The harmonic content was dominated by lower order harmonics, which is relevant for the design of harmonic filters and STATCOM compensation.

Keywords: Offshore wind power, voltage, harmonics, export cable, grid strength, power electronic device.

Preface and acknowledgements

This master's thesis was conducted during the spring semester of 2023 at the GQPS System Design department at Hitachi Energy Sweden AB in Västerås, in collaboration with the Division of Electric Power Engineering at Chalmers University of Technology. The thesis was presented on the 15th of June 2023, with final revisions completed in May 2026.

Throughout the project, the GQPS department provided regular follow-ups, technical discussions on the PSCAD model and simulation setup, and review of intermediate results. The discussions and feedback from this collaboration shaped the direction of the work and the interpretation of the results.

I would like to thank my supervisor at Hitachi Energy, Emil Lindström, and my examiner at Chalmers, Massimo Bongiorno, for their input throughout the project.

Gabriel Hassellöf, Västerås, May 2026

List of Acronyms

Below is the list of acronyms that have been used throughout this thesis:

BTB Back-to-back.

DFIG Doubly fed Induction Generator.
DFT Discrete Fourier Transform.

FFT Fast Fourier transform.
FRT Fault Ride-Through.

GFL Grid Following.
GFM Grid Forming.
GSC Grid side converter.

HVAC High-voltage Alternating Current.

IGBT Insulated Gate Bipolar Transistor.

OLTC On-load Tap Changer.
ONSS Onshore Substation.
OSS Offshore Substation.
OWPP Offshore Wind Power Plant.

PCC Point of Common Coupling.
PED Power Electronic Device.
PWM Pulse-width Modulation.

RMS Root Mean Square.
RSC Rotor side converter.

SCR Short Circuit Ratio.
$\mathbf{S_{sc}}$ Short circuit apparent power.
STATCOM Static Synchronous Compensator.
SVC Static Var Compensator.

THD Total Harmonic Distortion.
TSO Transmission System Operator.

VSC Voltage Source Converter.

WPP Wind Power Plant.
WTG Wind Turbine Generator.

Contents

List of Figures

List of Tables

1
Introduction

Voltage harmonics can result from the operation of power electronic devices (PEDs). The harmonics can interact with the main grid, exciting resonances and producing harmonic distortion that exceeds allowed limits. Wind power is a renewable power source that uses PEDs, which can introduce harmonics into the grid. This thesis aims to investigate the impact of offshore wind power in terms of voltage harmonics and harmonic impedance seen from the main grid. The objective is to gain a better understanding of what affects offshore wind power plants' (OWPPs) feasibility, and how it potentially could interfere with voltage regulating equipment, such as STATCOMs, produced by companies like Hitachi Energy.

1.1 Background

With renewable power generation such as type IV wind power making up a larger share of the power generation in the grid and replacing conventional generation, such as nuclear power, new demands are placed on the grid. Converter based generation lacks benefits that are present in synchronous generation, such as inertia, that provide stability features, and come with challenges like harmonic resonance and flicker. To mitigate some of the drawbacks of converter-based generation, power quality equipment such as STATCOMS can be used. Moreover, as the wind turbines are using PEDs in order to convert from the turbines' frequency to match the main grid's frequency, voltage harmonics are introduced, which may interfere with the main grid and power quality equipment.

Voltage harmonics excite resonances formed by the capacitive and inductive elements in the grid, and the resulting amplification will have a negative impact on the grid stability. Weak grids are extra vulnerable to this, as the amplified harmonics can harm equipment and devices in the grid, and cause false tripping. This can in turn result in blackouts or higher operational cost of components in the grid, due to an increased maintenance need.

Resonances in the system arise as a result of interaction between capacitive and inductive elements. Examples of these elements are cables, filters, capacitor banks and transformers, all of which are becoming greater in size as the OWPPs increase in size. These become problematic when they coincide with harmonic frequencies in the grid.

The voltage harmonics must be considered in order to meet requirements on harmonic distortion, and also be regarded in the design and operation of a STATCOM connected at the PCC. Harmonics already present in the main grid also risk adding with the harmonics

introduced from the OWPP, meaning that the existing harmonic content of the main grid also affects the feasibility of establishing an OWPP.

In order to investigate some of the factors affecting the harmonic impact of establishing an OWPP, this thesis analyzes the harmonic content up to the 63rd order by simulating a few cases where the conditions of the system are changed in a PSCAD model of the power system, comprised of an OWPP connected to a main grid. The factors include: the export cable length from the OWPP to the main grid, a stronger and weaker main grid, and lastly, harmonics already present in the main grid. The report also covers the main components of OWPPs and theory related to harmonics.

1.2 Aim

To shed light on the matter and prioritize the challenges affecting OWPP feasibility, and thereby support the ability to integrate more wind power into the grid, the thesis aims to answer three questions related to harmonics, which make up one of the greater challenges with OWPP generation. Specifically, the thesis quantifies how grid strength, HVAC export cable length, and the order of injected voltage harmonics affect the voltage harmonic distortion and harmonic impedance seen at the PCC.

1.3 Research questions

To address the aim above, this thesis investigates the following research questions:

- How do shorter/longer HVAC cables impact the voltage harmonic distortion and harmonic impedance at the PCC?
- How do stronger/weaker grids impact the voltage harmonic distortion and harmonic impedance at the PCC?
- How does the order of harmonics injected from the main grid affect the voltage harmonic distortion and harmonic impedance at the PCC?

1.4 Scope

Below states what is to be included in the thesis, as well as elements that are not covered.

- Confidential and competitive information for Hitachi Energy Sweden AB will not be presented in the thesis. This means certain parts of the model, like the wind farm, are not described in detail. Sufficient parameters are provided for the methodology to be understood and the results interpreted, even if exact reproduction is not possible.
- The simulations will be conducted in PSCAD, and the data treated and analyzed in MATLAB.
- Only harmonics up to the 63rd order are analyzed.

- The reactive part of the harmonic impedance is not analyzed in detail. The reactive component was inductive in the example case shown in section 4.2.1, and the other cases showed the same behavior. The resistive component is the focus of the analysis, while a full analysis of the reactive component across all cases is left for future studies (see section 5.7).
- The simulated wind farms will be of type IV using grid following (GFL) converters.

1.5 Methodology

The main methods used were a literature study and simulations. The literature study covered OWPP topology, harmonics in PED-based generation, grid strength, and reactive power compensation, which provided the foundation for the simulated scenarios. The simulations were performed in PSCAD using an aggregated type IV OWPP model, provided by Hitachi Energy AB. The time domain output was analyzed in MATLAB through FFT to obtain the harmonic content at the PCC. Three factors were varied in the simulated cases: grid strength, export cable length, and the order of the injected voltage harmonic. Both methods are described in detail in section 3.

1.6 Ethics and sustainability

Offshore wind power plays a role in the transition away from fossil-based generation by exploiting the stronger and more consistent winds available at sea, while not being in peoples' backyards. Integrating it into the existing grid comes with challenges that go beyond technical feasibility alone. This section briefly discusses the societal, ethical, and ecological aspects of OWPPs, with a focus on how they relate to the harmonic distortion subject of this thesis.

1.6.1 Societal impact

Having access to electricity is vital for a functioning society, and OWPPs help meet a growing demand for power as electrification takes place, and does so with a low carbon emission footprint. This contributes to the UN Sustainable Development Goal 7 of affordable and clean energy [1]. However, the impact of implementing OWPP goes beyond just impacting the wind farm operator. As described in section 2.5, harmonic distortion at the PCC can degrade equipment, cause measurement errors and trigger false tripping, all of which carry costs and can deprive consumers of access to clean energy.

Ensuring harmonic compliance according to the grid codes is therefore of societal concern. The findings in this thesis, particularly the importance of grid strength in order to limit THD, are directly relevant to where new OWPPs can be installed, and what grid reinforcement the surrounding society needs to plan for.

1.6.2 Ethical impact

The construction and operation of OWPPs comes with safety challenges that are different in comparison to onshore generation, with workers facing remote worksites, tough conditions and challenging environments for emergency services, putting personnel at potentially fatal risk [2]. Conducting thorough engineering studies before construction, including the analysis of harmonic distortion impact, supports the reduced need for costly modifications and risk for the workers conducting the modifications or maintenance.

From a research point of view, the simulations performed in this thesis are based on a simplified, aggregated model of an OWPP. The limitations of the model, particularly the inability to capture converter switching harmonics, are stated openly in sections 5 and 4 to avoid assumptions and give other researchers a fair basis to build on. Several directions for future work are also identified in section 6, providing concrete starting points for studies that could address the limitations of the present model.

From a data integrity perspective, each simulation case in this thesis was run once and analyzed using a single FFT window, with the limitations of this choice acknowledged in section 5.6. The model was provided by Hitachi Energy under a confidentiality agreement, which essentially makes the converter and wind farm parameters a black box. These constraints are stated openly in the scope (section 1.4), so that the results can be evaluated within the limits of what was reproducible.

1.6.3 Ecological impact

OWPPs replace fossil-based power generation, and therefore reduce CO_2 emissions throughout their operational life, but they are not without ecological impact. Construction can disturb marine life such as fish and mammals, and the turbines themselves can strike birds that are migrating [3]. It should be mentioned that OWPPs also come with benefits, like fish creating artificial reefs and being protected from fishing trawlers [4].

Submarine cables, which play a big role in this thesis, also contribute to the ecological impact by disturbing the seabed during installation. Designing OWPPs so that they fulfill the grid code requirements without needing oversized and over dimensioned equipment helps to reduce the emissions during manufacturing, and also reduce the physical footprint, which is a practical reason for understanding harmonic behavior at the PCC.

1.7 Report structure

The report has six sections. Section 1 gives context for the thesis and sets the foundation of the investigation. Section 2 provides knowledge on OWPPs, and methods and tools needed to analyze and interpret the results, based on the literature study. Section 3 describes the parameters varied in the simulated model and how the data was gathered and treated. Section 4 presents the results of the simulations. Section 5 provides a discussion of the results and what could be improved and explored in future studies. Section 6

concludes the results found in the thesis.

2
Theory

The purpose of the theory section is to give a background to understand the methodology section and results of the thesis. It describes the basics of OWPPs and some properties of the grid.

2.1 Offshore wind power plants

Wind turbines installed offshore making up OWPPs are placed offshore due to wind speeds being more consistent and quicker compared to wind turbines located on land. The quicker wind speeds lead to increased power generation, making offshore installation more favorable compared to onshore installations [5].

OWPPs vary in production capacity but tend to increase in size. In 2002, the world's biggest wind farm Horns Rev 1 had a capacity of 160 MW [6]. 2012 the biggest OWPP in the world was the London Array with 630 MW [7]. One of the biggest OWPPs in the world is the Hornsea 2 OWPP with a capacity of 1.3 GW [8].

The following subsections go through the main components that make up the OWPP.

2.1.1 Wind turbine types

There are different ways to generate power from wind turbines, and the main types are named type I-IV. The most common type of generator is a doubly fed induction generator (DFIG), type III, but synchronous generators (SG), type IV, specifically permanent magnet synchronous generators, are becoming the most popular type in new wind power plants [7]. For this reason, combined with the fact that there are fewer studies on type IV compared to III, type IV is studied in this report.

Fixed-speed turbines
The first type (I) is called fixed-speed turbine and uses a squirrel-cage induction generator, spinning at a certain speed varying roughly 1 % because of slip [9]. These generators come with challenges in case of faults, risking an increased absorption of reactive power which can risk a local voltage collapse, impeding voltage recovery [10].

Variable-speed turbines
Variable wind speed turbines (type II-IV) have a higher efficiency than fixed-speed turbines. The last two types are the most common ones, using PEDs.

Type II wind turbines use a wound rotor induction generator with a resistor in series with the rotor, which gives slip control and allows for a variable speed range of roughly 10 % [9].

Type III uses a doubly fed induction generator (DFIG) with a BTB-converter rated at 30 % of the generator power (partial-scale PED) that feeds the rotor windings with a controllable voltage. This enables the mechanical speed of the rotor to be decoupled from the synchronous frequency of the grid, allowing for variable-speed operation, and recovering slip-power [9].

Type IV uses a fully rated converter in series with the generator, which allows for full active and reactive power control within the limitations of the converter. The rotor side converter (RSC) of the BTB-converter is found at the rotor side, and the grid side converter (GSC) is found at the grid side, as depicted in Figure 2.1. The generator used depends on chosen design, either an induction generator or a synchronous generator, with permanent magnet synchronous generators becoming more popular due to its ability to control power fully by not requiring slip rings and brushes, which is appropriate for offshore conditions where minimal maintenance is favorable [7], [9].

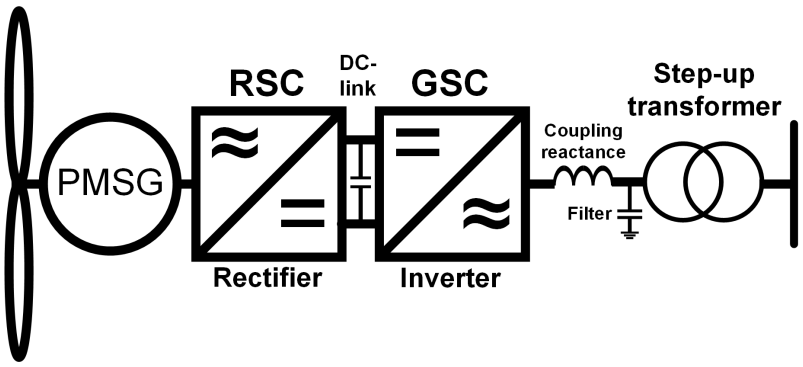

Figure 2.1: A model of a type IV WTG.

2.1.2 OWPP topology

The offshore wind power plant (OWPP) consists of numerous components and modules. When the wind drives the blades, the main shaft within the nacelle, which houses all the generating equipment, begins to rotate. Depending on the design of the wind tower, the shaft could be connected to a gearbox in order to get the desired rotational frequency for the generator. The generator is connected to a back-to-back (BTB)-converter in order to supply the grid with a desired frequency (50 Hz) and phase angle. A power transformer in the nacelle transforms the low voltage amplitude from the terminals of the converter up to a medium voltage, often 33 or 66 kV [11], [12].

The power is collected by inter-array cables, connecting the WTGs to the offshore substation (OSS). At the OSS, the voltage is transformed from medium voltage to high voltage to minimize losses when exporting the power to shore. At the OSS there is also the option to install filters and reactive power compensation before the power is transferred via a

submarine HVAC cable to shore.

Under the shore, the HVAC export cable often goes through a horizontal directional drilling. Onshore the cable is often directly connected to the onshore substation (ONSS). Before reaching the ONSS, the cable could be transition jointed at a transition station, where reactive power compensation is possible. At the ONSS, the voltage level either remains at the same level as in the export cable, or is transformed to a higher grid system voltage. A simplified model of the entire system is displayed below in Figure 2.2.

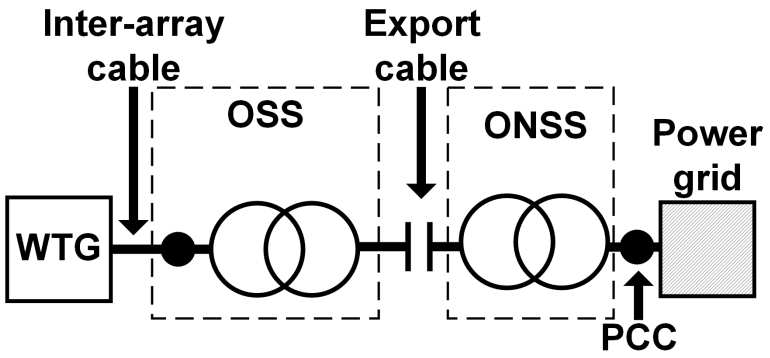

Figure 2.2: A simplified topology of an OWPP and its interconnection to the power grid.

To give some examples of existing OWPPs using HVAC, Table 2.1 lists a selection of OWPPs in northern Europe, with rated transmission powers from 50 MW up to almost 900 MW, and export cable lengths ranging between 32 and 136 km. Figure 2.3 visualizes the same OWPPs.

Table 2.1: Selected OWPPs using HVAC.

Wind farm	Country	Export cable length [km]	Power [MW] / no. cables	Voltage [kV]	Year
Horns Rev 2	DK	100	209/1	150	2009
Baltic 1	DE	77	48/1	150	2011
Greater Gabbard	UK	46	504/3	132	2012
London Array	UK	54	630/4	150	2012
Anholt	DK	85	400/1	245	2014
Riffgat	DE	80	113/1	155	2014
EnBW Baltic 2	DE	136	288/2	150	2015
Gemini	NL	110	600/4	220	2017
Horns Rev 3	DK	32	400/1	220	2018
Borssele Alpha	NL	61	700/2	220	2021
Kriegers Flak	DK	80	605/2	220	2021
Triton Knoll	UK	107	857/2	220	2022

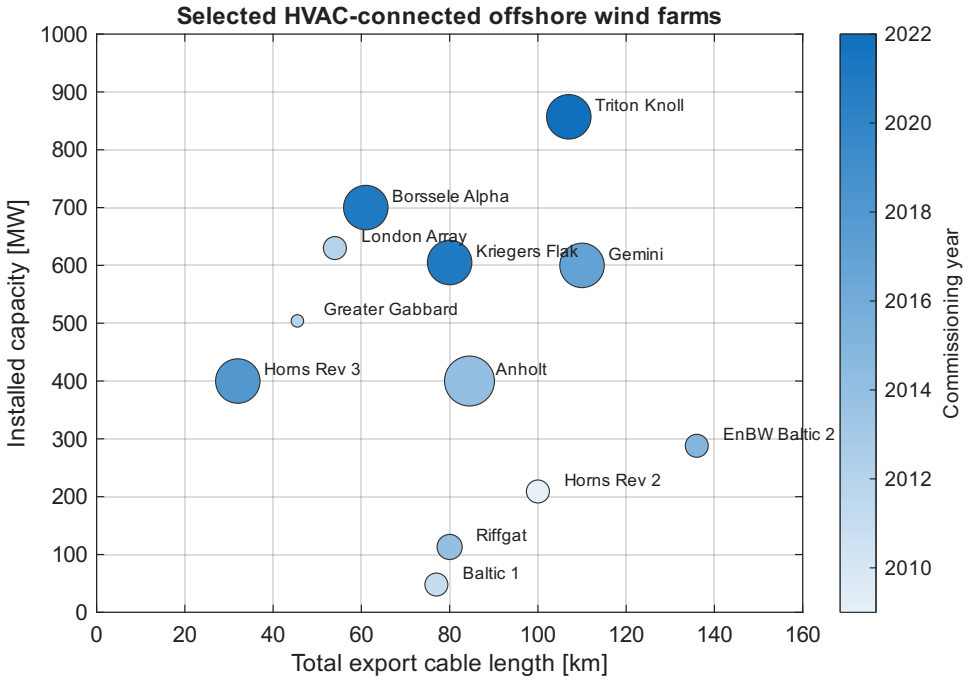

Figure 2.3: Installed capacity compared to total export cable length for the OWPP in Table 2.1. Greater marker size means greater export voltage, and the colormap indicates commissioning year.

2.1.3 Shunt reactors

Due to the nature of submarine cables being capacitive, there is a need for reactive power compensation, which can be achieved using shunt reactors [13], [14]. The shunt reactor is essentially an inductor, which absorbs reactive power for a leading power factor, resulting in a reduction of overvoltages specifically in situations of low loads [15].

The long export cables that are insufficiently shunt compensated can cause voltage surges due to reactive power output, under-excitation of synchronous generators and great temporary overvoltages may arise during load rejection and no-load energization. Furthermore, the current required for charging the cable (no-load current) might surpass the rated current of the circuit breakers [16], [17]. These issues can be solved by installing shunt reactors at the line terminals, which decreases the amount of reactive power supplied to the main grid while keeping the internal reactive power equilibrium of the cable [16].

2.1.4 Back-to-back converters

BTB-converters are essentially dual-voltage source converters connected through a DC-link, converting the voltage from AC to DC (rectifying), and back to AC (inverting). This is to transform the varying frequency and voltage from the generator to a constant frequency and angle that is appropriate for the main grid [9].

The RSC controls speed and torque of the generator, while the GSC controls the DC-link voltage and grid reactive power [13]. The converters in OWPP applications operate at a

switching frequency of 1-3 kHz to minimize switching losses and maximize power density [10]. The GSC operates at a low voltage level, e.g. 690 V [13].

If there would be a drastic grid voltage drop, the capability to transfer energy from the turbine to the grid would be impeded, which would mean an increase in DC-voltage of the BTB-converter and the wind turbine would spin faster [9].

While the PEDs offer more opportunities to optimize electrical design in terms of power quality, grid code requirements, handling of faults and grid support, they also require an intricate and meticulous design that addresses harmonic distortion, stability, and resonance behavior [18]. This is because PEDs use semiconductors that exhibit nonlinear behavior in terms of voltage and current, creating harmonics. This can result in problems like overheating of power cables, overloading of transformers and motors, reduction of the power factor (reduction of transferred power) and unintentional tripping of protective relays [19].

The harmonics originating from the BTB-converter are from the switching transients in the non-linear inverter [20], [21]. When part of a larger system that has frequency-dependent components, the harmonics can excite resonances in the network, resulting in amplified distortion that can damage other equipment in the grid. This equipment could for example be a STATCOM which could have its performance negatively affected.

The BTB-converters mentioned in this thesis are typically grid-following (GFL) converters. GFL converters are used as controllable current sources to supply the grid with a desired amount of reactive and active power. To achieve this, the power controller has to be synchronized with the grid voltage (frequency, phase angle and amplitude) to follow the grid [22]. There are also grid-forming converters (GFM) that work by having the converters acting as voltage sources instead of current sources and basing the synchronization on the transfer of active power and the swing equation [23].

The distinction between GFL and GFM is relevant for harmonic studies, as the two interact with the surrounding grid impedance in different ways. A GFL, acting as a controllable current source, will inject harmonic currents that result from its modulation, and the resulting harmonic voltage at the PCC depends on the grid impedance for respective frequencies. A strong grid will attenuate the voltage distortion, but a weak grid will amplify it [23].

A GFM converter on the other hand, behaving as a voltage source behind an impedance, sets the voltage at its terminals, and the harmonic current is then determined by the difference between this voltage and the surrounding grid voltage divided by the converter's output impedance. This means that GFM converters are better suited for weak grids and for acting more like generators that provide inertia [24].

The simulations in this report use GFL converters, which means that the harmonic results reflect the GFL response, and may not apply directly to GFM-converters GFM-converters.

2.1.4.1 WTGs and harmonics

The output voltage of the GSC is usually filtered before supplying the step-up transformer. With several converters connected to the grid, there is a risk that the voltage distortion might surpass the limits specified for the PCC. The GSCs typically use a pulse-width modulation (PWM) strategy that switches at a fixed switching frequency. The interaction between the fixed frequency of the power grid and the switching frequency of the double-edge naturally sampled PWM results in the generation of harmonics in the output voltage of the three-phase network bridge [13].

Because of the DC-link isolating the generator side from the grid side in the circuit, the harmonics generated by the rotor side converter (RSC) are insignificant on the grid side [13].

2.2 Submarine cables

There are two main types of cable used in OWPPs, export cables that connect the OSS to the ONSS, and inter-array cables that connect the individual WTGs to the OSS. Export cables vary in length depending on where the OWPP is situated. To exemplify, one OWPP is located 15 km offshore, an investigation for submarine cable routes for a future OWPP uses lengths of 18-150 km, while another OWPP is located 89 km offshore and one OWPP has a 100 km HVAC export cable [8], [13], [25], [26].

Individual inter-array cables are shorter than export cables, but due to the number of WTGs used, the total length of the inter-array cables adds up. One OWPP has 165 WTGs with 165 inter-array cables with a combined length of 374 km [27]. The voltage of the inter-array cables is lower than the export cable [26], [28].

For studies in the frequency domain, AC cables are often represented using a lumped Pi-section model, where the total series resistance R and inductance L are lumped in the model, and the total shunt capacitance is split on each side of the cable, connected in shunt, as in Figure 2.4.

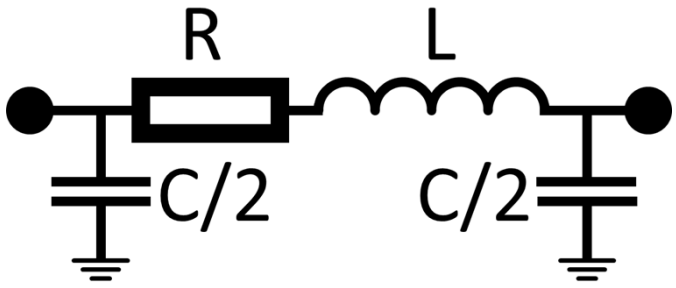

Figure 2.4: Example of a π-section.

The series and shunt reactances of the cable are frequency dependent and are given by

$$X_L = 2\pi f L \tag{2.1}$$

$$X_C = \frac{1}{2\pi fC} \tag{2.2}$$

where f is the frequency, L is the total series inductance, and C is the total shunt capacitance of the cable.

With increased cable length, the capacitance of the cable naturally becomes greater, which pushes the resonance down to a lower frequency [29], [30]. This shifts the system's resonance into the range of harmonic orders typically present in the network, increasing the risk that harmonics will be amplified by the resonance between the cable capacitance and the inductance of components such as transformers [19]. This relationship can be expressed as

$$f_{res} = \frac{1}{2\pi\sqrt{LC}} \tag{2.3}$$

where L is the total inductance of the upstream system (transformers and grid impedance) and C is the cable's shunt capacitance, showing that an increase in C lowers resonance frequency f_{res}.

A cable produces reactive power according to

$$Q_{cable} = E^2 \cdot 2\pi fC \tag{2.4}$$

where f is the frequency, C is the capacitance and E is the line-to-line voltage [31]. Since the cable capacitance accumulates with length, and the reactive power scales with the square of voltage, long HVAC cables produce significant reactive power which needs to be compensated, typically by shunt reactors.

Since submarine cables are expensive and technically challenging to repair, it is crucial to ensure that their lifespan is long, hence the need to prevent overheating and harmonics in the cable [32], [33].

The most common reason for a short circuit in submarine cables is due to insulation breakdown, meaning that there is a disruption in the insulation between the conductor supplying power and the seawater, interfering with the power flow between two power stations. The insulation breakdown can have many different causes: damage from anchors, ambient temperature and most significantly aging and water treeing [34].

The submarine HVAC cables are three-core cables that comes with the advantage that magnetic fields are cancelled out due to symmetry. They can also house cables for integrated communication. The con of the three-core cables is that they have complicated cable joints, are harder to handle compared to single-core cables, and in case of damage, the entire cable needs to be replaced [35]. For cables, there is also a risk of reflection at the cable terminals. These reflections might cause standing waves that shift resonant frequencies of the cable system [36].

2.2.1 Power transformers

The purpose of power transformers is to increase the voltage in order to minimize losses when transferring power. Due to leakage inductance between the transformer windings,

the transformers function as first-order low pass filters [37].

At the ONSS, there is an on-load tap changing (OLTC) transformer, transforming the voltage from the WTGs to the voltage used in the export cable. The transformer is wye-delta transformer with a grounded wye winding. The grounding enables a route for ground fault zero-sequence currents. The grounding transformers can also restrict the magnitude of the ground fault current [38]. This way of connecting allows for the use of single-phase devices on the wye-side, while not requiring four conductors on the primary side [39].

In the case of triplen harmonics (3rd, 9th, 15th, etc.) reaching the wye-side of the transformer, the delta windings allow for circulation of the harmonic currents, but they will be confined within the delta windings and not appear as line currents on the secondary side. This is because triplen harmonics are zero-sequence components, meaning the three phases are in phase with each other at these frequencies, and a delta winding provides no external return path for zero-sequence currents [40].

Since wind power generation is stochastic, the current through the inter-array cables is continuously changing and hence the voltage at the low voltage side of the transformers [41], [42]. In the case of extreme voltages (low or high), the protection system might activate the protection system of the wind turbines or the bigger inter-array network. To regulate the voltage at the low voltage side of the OLTC transformers, a tap changer is used to mechanically adjust the turn ratio during load while ensuring uninterrupted power flow. The tap changer is usually located at the high voltage winding side because the current is lower which allows for more compact design [42].

At the ONSS there is an isolating transformer connecting the OWPP to the PCC. The isolating transformer is a wye-wye with ground at both sides. The isolating transformer has a unity turns ratio, meaning the same voltage on both sides. The transformer decouples the two sides from each other [43].

2.3 Electrical networks

This section covers two important grid properties that directly affect how an OWPP behaves: the strength of the grid at the PCC, and the grid codes that define the requirements an OWPP must meet to operate in the first place.

2.3.1 Grid strength

Grid strength is a metric to convey the capability of a power system to uphold its essential characteristics: voltage and frequency during interactions with a connection during all operational circumstances. Grid strength is relative, and both the system characteristics at the connection point and the size of the WPP need to be considered. Two systems with different production active power capacity connected to the same point might have different grid strengths [44].

For components, grid strength can be determined by the short circuit ratio (SCR), which is dependent on the short circuit apparent power (S_{sc}) and the rated apparent power of the connected device S_n, which can be seen in (2.5). The S_{sc} decreases with greater impedance as seen in (2.6), which means that for longer lines, the grid is generally weaker. Numerically, a SCR greater than 5 corresponds to a "strong" grid, a SCR below 5 corresponds to a "weak" grid and a SCR below 3 corresponds to a "very weak" grid [44].

$$\text{SCR} = \frac{S_{sc}}{S_n} \tag{2.5}$$

The S_{sc} can be calculated according to

$$S_{sc} = \frac{|E|^2}{Z_{grid}} \tag{2.6}$$

where E is the line-to-line voltage and Z_{grid} is the Thevenin equivalent impedance of the grid, consisting of a resistance followed by an inductance in series. It can be calculated using

$$Z_{grid} = \sqrt{R_{grid}^2 + X_{grid}^2} \tag{2.7}$$

where R_{grid} is the equivalent grid resistance and X_{grid} comes from the equivalent grid inductance, assuming the reactance is purely inductive.

The challenge with OWPPs is that they often are located far away from the consumers, meaning more grid impedance compared to an OWPP located close to consumers. This brings the S_{sc} down, meaning a lower SCR. A countermeasure is to increase the voltage, but eventually the voltage transformation becomes too expensive [45].

The S_{sc} can also be calculated as

$$S_{sc} = \sqrt{3} * |E| * |I_{sc}| \tag{2.8}$$

,where I_{sc} is the short circuit current.

The transmission line reactance to resistance ratio (X/R-ratio) is a grid strength parameter that affects the current flow. A lower X/R-ratio limits the I_{sc} flow, resulting in lower S_{sc} and hence a weaker grid [46]. The X/R-ratio also affects the grid's dampening capabilities [46]. As mentioned in Section 2.4.7, weak grid connections are typically associated with higher levels of harmonic distortion [47].

2.3.2 Grid codes

Grid codes are sets of requirements and rights imposed by the TSOs for loads and generators in the transmission system, including OWPPs [48]. Grid codes set the requirements

for the generation to be connected, to ensure that efficient, safe, and financially feasible operation of the transmission or distribution system is possible [49].

The OWPP interconnection must meet the requirements stated in the grid codes, which include feeding the grid with a current that has a low total harmonic distortion (THD), supplying sufficient reactive power to grid upon request from the TSO, ride through faults and supporting frequency and voltage regulation [9]. The voltage level regulation can be required to perform by changing the power factor and hence controlling the reactive power transferred [45], [50], [51].

Countries with large amounts of wind power generation, or countries with weak grids usually have more strict grid codes, which puts higher requirements on active and reactive power responses during and after faults in the system. Active power response regulations ensure that the system maintains short-term frequency stability, while reactive power support provided by the WPP can strengthen the voltage stability limits of the system [48].

One example of a grid code and some of its requirements is the UK TSO National Grid Electricity System Operator's "THE GRID CODE" issue 6 [52], which, like many other grid codes, requires a reactive power factor between 0.95 leading and 0.95 lagging. Furthermore, "THE GRID CODE" allows for the frequency varying from 47.5 to 52.0 Hz (although it requires a certain operation period depending on what frequency is reached).

Another example of a requirement from "THE GRID CODE" is the specified nominal voltage levels, where for 275 kV, it's allowed to operate within $\pm 10\,\%$ of that. While grid codes might specify THD limits for example, "THE GRID CODE" refers to bilateral agreements and recommendations by other associations, like the Energy Networks Association's "Engineering Recommendation G5/5", which states THD limits for different voltage levels and how they shall be measured using IEEE standards [53].

These strict grid code requirements on aspects such as power quality and harmonic distortion form the basis of this work, which investigates harmonic behavior under various scenarios to support grid code compliance.

2.4 Power quality

OWPPs are vulnerable to harmonic distortion due to the large submarine cable network, which introduces resonances that can amplify harmonic injections, combined with the risk of low available short-circuit power at the grid interconnection point, posing a threat to the operation of the WTG controller [30]. To ensure normal operation and prevent harmonic distortion, the following sections explore some important aspects of power quality.

2.4.1 Harmonic, harmonic distortion, and resonance

Before describing the specific phenomena, it is useful to clarify three terms that are often used interchangeably, but mean different things. A harmonic is a sinusoidal component at

an integer multiple of the fundamental frequency, and is a property of a signal. Harmonic distortion is the resulting deviation of a voltage or current waveform from a pure sinusoid, caused by the presence of harmonics, and is quantified by the total harmonic distortion (THD) defined later in this section. Resonance is a property of a system, not of a signal, occurring at frequencies where inductive and capacitive reactances cancel each other out, and the impedance becomes either very high or very low. At a resonance frequency, even small harmonic currents can produce large harmonic voltages, so the harmonic distortion observed at a given point in the network depends on both the harmonic injection, and the resonance behavior of the surrounding network [54].

2.4.2 Voltage harmonics

The voltage waveforms in power systems are ideally purely sinusoidal with a constant magnitude and frequency to meet customer demands. When there is a deviation from this throughout one period of the cycle of the grid frequency, it is called a harmonic distortion [55].

Harmonic distortion is unavoidable in the power system due to use of nonlinear loads and generators like PEDs. Resonances have high Q (quality factor) and can be excited by even small harmonic currents from the PEDs or their control [18]. Resonances occur at frequencies where the inductive and capacitive reactances of the system are equal in magnitude, causing the impedance to become very high or very low [55],

Since smaller disturbances can be amplified by these resonances, normal operations might be jeopardized, and instability can occur. For this reason, amplification from series and parallel resonances needs to be considered to avoid compromised operation, degradation, or even irreversible damage [18]. The harmonic distortion can also result in overvoltages, which can cause the protection system to disconnect the WTGs [30].

Further, harmonic distortions can result in the following [18]:

- Decreased generating- and transmission efficiency.
- Aging of insulation due to voltage or temperature stress.
- Measurement errors from devices that are made for measuring sinusoidal voltages and currents.
- Failure of protective devices.
- Warming and vibrations of all components in the power system, with some elements, such as transformers and reactors, being especially susceptible to these issues.

When a transformer is energized, lower order harmonics up to the 13th order can be generated. Harmonics can also be generated in transformers during normal operation since they often operate close to their magnetic saturation point. This is due to the nonlinear correlation between voltage and current at this point, especially in overvoltage situations [55]. Odd harmonics often come from overexcited transformers, but in case the transformer has delta-windings, the triplen harmonics will be blocked [55].

2.4.3 Sequence components

A balanced three-phase system can be decomposed into three symmetrical components: positive, negative and zero sequence [56]. Positive-sequence components are three phasors of the same magnitude, 120° apart, rotating in the same direction (A-B-C). Negative-sequence components also have equal magnitudes 120° apart, but rotate in the opposite direction (A-C-B). Zero-sequence components consist of three phasors of the same magnitude that have no shift between them, and hence are in phase with each other [57].

Sequence components are also widely used for fault analysis, where unbalanced faults like single-phase-to-ground or phase-to-phase result in a mix of positive, negative and zero sequence currents. In this thesis, however, sequence components are relevant only for understanding how harmonics of different orders propagate through the network.

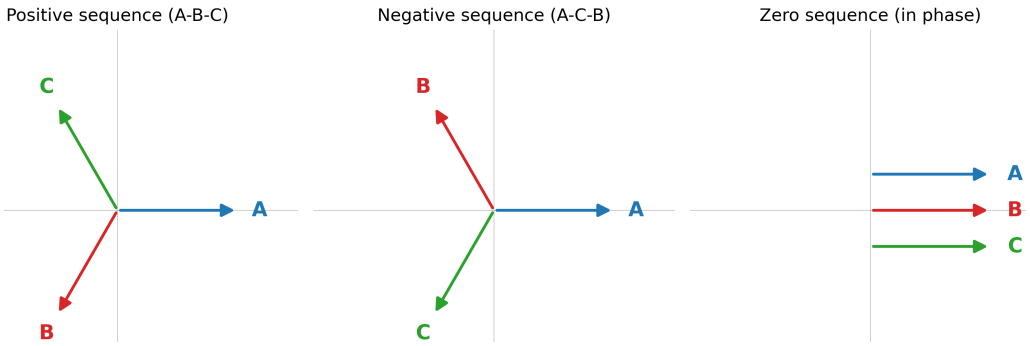

Figure 2.5: Phasor representation of the three symmetrical components in a balanced three-phase system. Positive sequence (A-B-C), negative sequence (A-C-B), and zero sequence (three aligned phasors).

This decomposition has direct implications for harmonics. In a balanced three-phase system, phase B is delayed from phase A by 120° at the fundamental frequency. At the h-th harmonic, the same physical time delay corresponds to $h\times$ 120° of the harmonic's own cycle.

For h = 5, this becomes 5 × 120° = 600°, which is equivalent to 240° (or -120°) after removing the full 360° rotations. This means that at the 5th harmonic, phase B is 120° ahead of phase A, reversing the phase rotation from A-B-C to A-C-B, which is the negative sequence, as seen in Figure 2.5 [57].

For h=3, the same calculation gives 3 × 120° = 360°, equivalent to 0°. All three phases are in phase with each other, which is the zero sequence, as seen in Figure 2.5.

- Harmonics of order $3k+1$ (1^{st}, 4^{th}, 7^{th}, 10^{th} ...) are positive sequence.
- Harmonics of order $3k-1$ (2^{nd}, 5^{th}, 8^{th}, 11^{th} ...) are negative sequence.
- Harmonics of order $3k$ (3^{rd}, 6^{th}, 9^{th} ...), called triplen harmonics, are zero sequence.

The sequence of a harmonic affects how it propagates through the network. Positive- and

negative-sequence currents sum to zero across the three phases and pass freely through three-phase equipment. Zero-sequence currents on the other hand, are in phase with each other and therefore add up. They require a return path, either through a neutral conductor (a fourth conductor), through a connection between the neutral point of a wye winding and ground, or through both. A delta-connected winding has no neutral point and therefore no path for zero-sequence current to exit to the line side, which is why triplen harmonics generated on one side of a delta-wye transformer are largely contained [40], [57].

2.4.4 Characteristic harmonics

In a balanced three-phase system where the voltage and current waveforms have the same shape and are shifted by $\pm$ 120° of the fundamental period, there will be characteristic harmonics. These characteristic harmonics are determined by the switching pattern used and the converter topology [13]. For three-phase converters, the dominant characteristic harmonics come at frequencies $6n \pm 1$ (particularly 5 and 7), where n is a positive integer [58].

The converters are using insulated gate bipolar transistors with high frequency PWM techniques, the harmonics components generated are of high order, near and beyond the switching frequency [10], [13]. With switching frequencies in the thousands of Hz, the main characteristic harmonics needed for consideration from the converter are $f_{gc} \pm 2f_e$, where f_{gc} is the grid side converter (GSC) switching frequency and f_e is the fundamental frequency of 50 Hz. For this reason, there should be significant harmonics at the 38th and 42nd order when using a switching frequency of 2 kHz [59]. Other papers use switching frequencies at 2 ± 1 kHz [13], [55], [60], [61]. In [55], the most significant harmonic was the 19th, which was generated by the PWM switching in the converters.

2.4.5 Non-characteristic harmonics

Unlike the characteristic harmonics, the non-characteristic harmonics are not determined by the modulation technique nor converter topology, but the grid condition (e.g., impedance characteristics, grid configuration, available generation and instantaneous load) and operating point of the converter [13]. For example, voltages in the AC system are always unbalanced and distorted to some extent and the system impedances, particularly in the converter transformer, are not precisely equal in all phases. This becomes more apparent during low load due to a naturally occurring greater imbalance [54].

Due to the variability of the grid system frequency, the frequency ratio may not necessarily be an integer. This means that the harmonic components generated from the GSC may not be multiples of the grid frequency, making it difficult to categorize the harmonic components as either characteristic or non-characteristic [13].

2.4.6 Harmonic filters

In order to mitigate harmonics and ensure that the voltage distortion at the PCC is within the grid code limits, harmonic filters can be utilized. Harmonic filters can be placed at many locations in the OWPP, for example at the AC-side of the converters, the ONSS, and

at the OSS after the export cable termination [25], [30], [62]. Filters come in two main types, active and passive:

Active filters are electronic devices that can supply current of the opposite phase to cancel out a wide range of harmonics and do this by performing reactive power compensation to regulate the voltage level. Passive filters are passive and can only cancel out specific harmonics and can consist of passive components such as inductors, capacitors, and resistors [63].

Passive filters lack flexibility and cannot be easily retuned in size or frequency when installed. This makes them ill-suited for dynamic system conditions [64]. Active filters have the ability to filter harmonics simultaneously, and modular active filters enable scalability of the filter without the need for supplementary drilling and wiring [65].

2.4.7 Total harmonic distortion

The level of distortion present in a waveform is often measured by assessing its total harmonic distortion (THD). The parameter describes the ratio between the RMS magnitude of all harmonic components and the RMS magnitude of the fundamental component, which can be seen in (2.9). For a high-power transmission system, the THD is usually <1 %, but for locations further away, like in the distribution system, it tends to be greater, particularly for weak grid connections [47].

The THD of the voltage is calculated using

$$\mathrm{THD} = \frac{\sqrt{\Sigma_{h=2}^{n} V_h^2}}{V_f} \tag{2.9}$$

where n is the highest harmonic analyzed, h is the harmonic order, V_f is the fundamental voltage harmonic and V_h is the voltage harmonic of h order.

For a high-voltage system rated above 161 kV, IEEE Std 519-2014 specifies a maximum allowed voltage THD of 1.5 % [66]. In Sweden, the maximum allowed THD for voltages between 130 and 400 kV is 2 % [39].

2.4.8 Harmonic impedance

Harmonic impedance describes the impedance present in the system at frequencies other than the fundamental, and will determine how a harmonic current will translate into a harmonic voltage for a given point in the network, at the PCC. According to Ohm's law, a drop in harmonic voltage across an impedance is proportional to both the harmonic current flowing through it, and the impedance for that frequency. This means that the voltage distortion is a direct result of the harmonic impedance seen from the point of injection [19].

A low harmonic impedance at the PCC means that even though there might be significant harmonic currents, the resulting voltage distortions can be very small. A high harmonic impedance can amplify the very same currents into greater voltage harmonics. Because of this, the harmonic impedance across the frequency spectrum is a useful indicator to voltage THD when assessing harmonic performance, as it reveals which frequencies are the most susceptible to amplification in OWPPs [19].

2.4.9 Power factor

The power factor (PF) is the ratio between active power (P) and apparent power (S) as in (2.10) [50].

$$PF = \frac{P}{S} \tag{2.10}$$

By analyzing the instantaneous phase angle φ between the voltage and the current in the system according to (2.11)

$$\varphi = \varphi_V - \varphi_I \tag{2.11}$$

, the power factor PF can also be calculated according to (2.12) [67].

$$PF = \cos\varphi. \tag{2.12}$$

In a purely resistive circuit, the power factor is 1, because voltage and current are not lagging (shifted) in relation to each other. In systems exhibiting a substantial reactive power component compared to the active power, the power factor will be lower. Since it is desirable to minimize the reactive power component, the aim is to keep the power factor as reasonably close to 1 as possible, to transfer as little reactive power as possible. According to [45], the minimum required power factor for connection to the main grid is 0.95.

2.4.10 Reactive power compensation

Reactive power impacts both voltage stability and the power factor [68]. Effective reactive power compensation can therefore improve system efficiency and increase the active power transfer capacity of a given network [69]. There are several different reactive power compensation technologies, each with different characteristics relevant to OWPP application.

Shunt reactors are essentially large inductors connected in parallel to the network. They absorb reactive power and are mainly used to compensate for the capacitive reactive power produced by long submarine cables, particularly under low-load conditions where the cable charging current would otherwise drive the voltage upward [15], [16]. They are passive devices, providing fixed compensation that cannot respond dynamically to changing grid conditions.

Capacitor banks provide reactive power, and are often used to improve the power factor of inductive loads. They are passive like shunt reactors and are typically switched in discrete steps [69], which limits how finely the compensation can be adjusted.

Static VAR compensators (SVC) combine thyristor-controlled reactors with capacitor banks to provide variable reactive power compensation, meaning that they are active (not passive). These respond faster than mechanically switched compensation, but rely on the grid voltage being present and behave non-linearly, which can introduce its own harmonic distortion [69].

Static synchronous compensators (STATCOM) use a voltage source converter to deliver a fast, accurate, and continuously variable amount of reactive power to the grid (active compensation). This is achieved by adjusting the magnitude and polarity of the reactive component of the current flowing through the STATCOM [69]. STATCOMs offer better dynamic performance than SVCs and are increasingly used in modern OWPP installations, including those provided by Hitachi Energy.

The topology is shown in Figure 2.6. The voltage source converter (VSC) exchanges reactive current with the grid through a coupling transformer T and a series leakage reactance jX_T. By controlling the magnitude of V_{VSC} relative to V''_{system}, the STATCOM draws capacitive current I_{cap} (injects reactive power) when $V_{VSC} > V''_{system}$, and inductive current I_{ind} (absorbs reactive power) when $V_{VSC} < V''_{system}$. The VSC produces V_{VSC} by rapidly switching between the two terminals of a capacitor. The capacitor C_{dc} supplies the DC source and is sized to keep its voltage V_{dc} stable through the switching cycles.

Of these, shunt reactors and STATCOMs are the most prevalent in the OWPP literature reviewed in this thesis. STATCOM performance can itself be affected by harmonic distortion at PCC, which connects directly to the harmonic studies presented in this work.

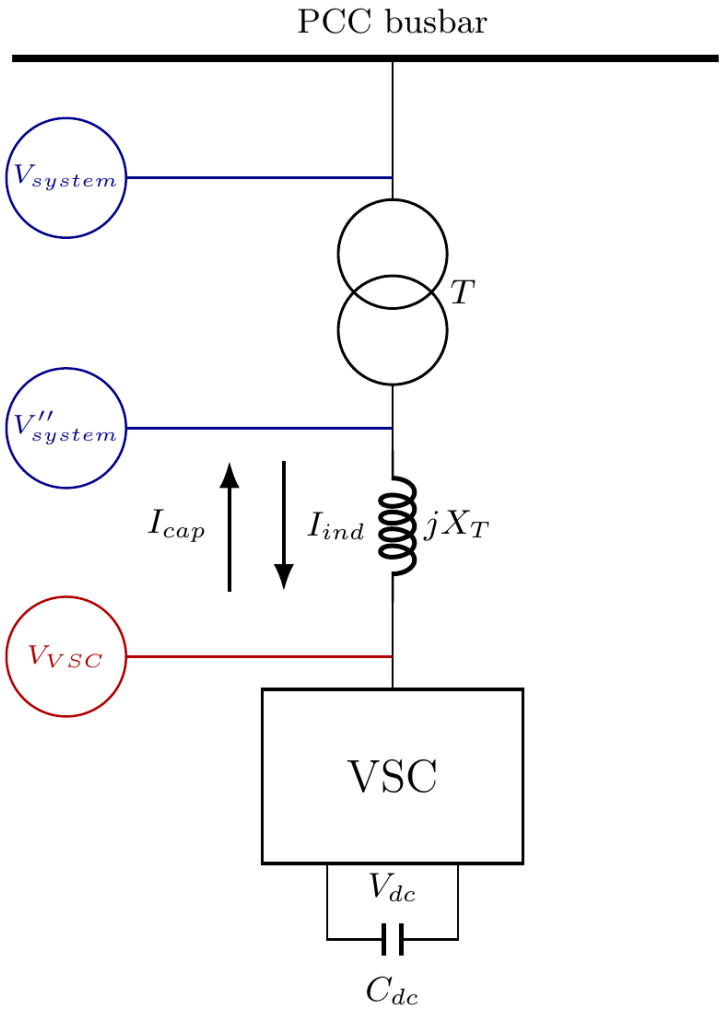

Figure 2.6: Topology of a STATCOM connected to the PCC, showing the VSC, coupling transformer T, series leakage reactance jX_T, and DC capacitor C_{dc}.

2.4.11 Interpreting harmonic impedance components

The harmonic impedance is comprised of two parts: resistance (real impedance) and reactance (imaginary impedance). To interpret some cases presented in the results, some of these conditions are explained here.

Negative resistance is counterintuitive, as a passive resistor always dissipates power and has a positive resistance. However, when measuring the impedance of an active system from the PCC, the entire system is measured (turbines, converters and other active equipment), not a passive component. Grid-following converters are designed to inject constant active power, and if the grid voltage drops, the controller increases its current output to keep $P = \mathrm{V} \times I$ constant. This is the opposite of how a resistor behaves, where a drop in voltage causes a drop in current.

For certain frequencies, this constant power control produces a relationship where current rises as voltage falls, which corresponds to a negative resistance for the measured impedance [70]. The energy comes from the wind, through the DC link, but seen from the grid side, the converter looks like a negative resistor in those frequency bands. Inverter-based generation is known to show this behavior in certain frequency ranges [71]–[73], and when the negative-resistance band of the wind farm overlaps with a resonance in the grid impedance, it can cause poor harmonic damping, steady-state errors, and instability [74].

Regarding reactance, a positive harmonic means that the total inductance is greater than the capacitance harmonic impedance for a certain frequency. If the harmonic impedance reactance is negative, it instead means that the capacitive harmonics are dominating in comparison to the inductive harmonics.

The impedance amplitude |Z| can be calculated using

$$|Z| = \frac{|V|}{|I|} \tag{2.13}$$

where V is the voltage harmonic, and I is the current harmonic. The real part of the impedance is calculated as

$$Z_{re} = |Z| * cos(\varphi) \tag{2.14}$$

where φ is the phase angle between the voltage and current, as in (2.11). The imaginary part of the impedance or reactance is calculated as:

$$Z_{im} = |Z| * sin(\varphi) \tag{2.15}$$

The reactive harmonic impedance will not be analyzed or presented other than a brief graph in section 4.2.1.

2.5 Impact of poor power quality in wind power plants

With the understanding of harmonics and wind farms comes the question of what happens when you combine them. The viability of the wind farm depends on safe and economically feasible operation, which can be directly hindered by poor power quality, particularly voltage harmonic distortion. This can both affect the OWPP, but also the surrounding grid, and hence come with expensive fines.

First, deterioration and reduced efficiency impact: Harmonic distortion accelerates the degradation of the components in the grid, like cables, transformers and reactors due to increased voltage and thermal stress [18]. This is particularly significant for submarine cables, whose repair is technically difficult and economically expensive, making lifetime optimization important [32], [33]. Moreover, distorted voltages and currents result in additional losses in transformers and rotating machines and reduced transmission efficiency [18], [19].

Second, the harmonic distortion can interfere with measurement and protection equipment. As these are made to measure on sinusoidal signals, significant distortions can result in measurement errors and false tripping [18], [19], which in the bigger picture can cause big grid disturbances.

Third, the harmonic distortion can affect power quality equipment such as STATCOMs or capacitor banks. These are designed for fundamental frequencies, and persistent unexpected harmonic currents can cause overheating and degrading [18].

Fourth, the mentioned effects will all be amplified in a weak grid. Weaker grids typically exhibit higher levels of harmonic distortion [47], and resonance peaks can amplify even small harmonics into significant distortion at PCC. As OWPPs often are connected at remote locations of the grid with limited short-circuit power, they are essentially weak grids by design.

Lastly, all of these aspects emphasize that the OWPP must comply with the grid code limits on harmonic emission and THD at the PCC. Failure to comply may result in costly operational delays, or the need for redesign or modification of compensating equipment, such as harmonic filters. Consequently, the harmonic behavior at the PCC directly impacts the feasibility of the entire OWPP.

3
Methodology

This section describes the methodology used in the thesis. Simulations were performed in PSCAD using a model of an OWPP provided by Hitachi Energy, which was modified to simulate an interconnected main grid of varying strength and with injected harmonics. Time domain data from the simulations was exported to MATLAB and analyzed in the frequency domain. The parameters and conditions of the PSCAD model, the data gathering and the treatment, are detailed in the sections below, with Figure 3.1 visualizing the main parts of the model.

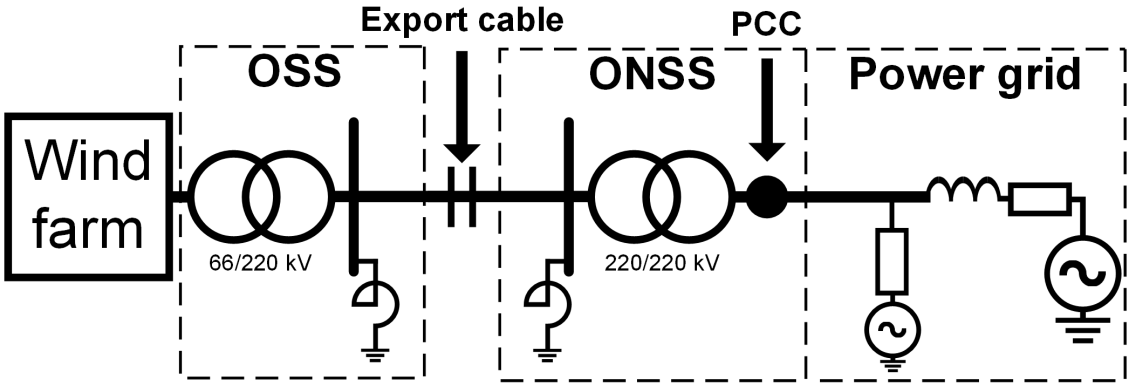

Figure 3.1: Topology of the main modules in the PSCAD model used for simulation.

3.1 Literature study

Throughout the master's thesis, research was conducted on OWPPs. Scientific papers and literature were primarily gathered from IEEE, and internal documents (such as specifications, workshops and studies) were provided by Hitachi Energy. The literature study gave answers to how the OWPPs are modelled, what components are involved and how individual components might affect and be affected by harmonics.

3.2 Modelling and parameter calculation

In this section, the main parameters and parameters being varied are described. The PSCAD model neglects the physical properties of the inter-array cables and does not model filters. This means that the generating wind farm is connected directly to the offshore transformer, without any consideration of inter-array cables.

3.2.1 Wind farm

The wind farm contains the aggregated turbines with a constant power of 360 MW, which is connected to an OLTC transformer which transforms the voltage from 33 kV to 220 kV.

3.2.2 Export cable

The cable parameters are taken from data sheets and other sources, from which the capacitive reactance X_C and inductive reactance X_L are derived. The three-core 220 kV HVAC cable resistance is set to 16.70 μΩ/m based on [31] and a conductor cross-section of 1000 mm^2 is assumed. X_C is set to 16.75 MΩ*m based on the cable capacitance in [75] when using the same conductor size mentioned above. X_L is set to 0.1938 mΩ/m as given in [75] for the previously mentioned conductor size.

The cable lengths of 50 km and 100 km were chosen to cover a typical range of HVAC export cables in existing OWPPs (as seen in Table 2.1, ranging 32-136 km), with 100 km reaching the upper end (where cable capacitance has significant impact), and 50 km representing a mid-length case.

3.2.3 Shunt reactors

For long submarine cables operating at voltages greater than 155 kV, compensation at both cable terminals should be used. This is to guarantee that the wind farm export is not constrained by the cable capacity, that the voltage variation between land and offshore remains within the acceptable range, and that the charging current of the cable is lower than the rated limit of the circuit breakers [76]. Using the equations presented in [77], the following parameters are calculated for two cable lengths and presented in Table 3.1: cable reactances X_C and X_L, the reactor inductance, the power factors when using compensation PF_{comp} and when not using compensation PF_{cable}. The parameters are tuned to achieve a compensated power factor PF_{comp} as close to 1 as possible.

Table 3.1: Calculated shunt reactor parameters for two cable lengths.

Length [km]	X_C **[MΩm]**	X_L **[mΩ/m]**	Q_{react} **[MVAr]**	L_{react} **[H]**	PF_{cable}	PF_{comp}
100	16.75	0.1938	116.5	1.3224	0.9458	0.9997
50			64	2.4072	0.9885	0.9997

3.2.4 Power grid

To simulate a situation where the main grid can vary in strength and also inject harmonics into the PCC that risk interacting with the harmonics from the OWPP, a custom circuit is constructed. A three-phase voltage source is connected in series with a resistance R_{grid} and inductance L_{grid} to simulate the properties of the grid as a Thevenin equivalent [78]. In parallel to this, harmonic generator is placed, which is comprised of a three-phase voltage source placed behind a resistor, see Figure 3.2. The purpose of the harmonic generator is to introduce harmonics and analyze how they interact with the OWPP harmonics and

cable.

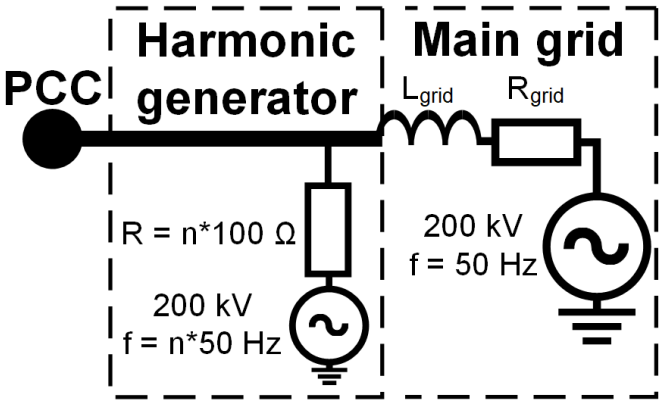

Figure 3.2: Grid model with harmonic generator of order n (left), and Thevenin equivalent of the main grid (right).

Two grid strengths are considered using different values of I_{sc}, where a greater I_{sc} results in greater S_{sc}, which is correlated to grid strength as seen in (2.6) [79]. The SCR is not calculated in this thesis. Calculating the SCR would require fixing a specific rated apparent power S_n for the OWPP, adding a parameter that is not relevant to the relative comparison this thesis aims to make.

Since S_{sc} is set differently in the two grid cases while all other parameters are kept constant, the resulting SCR values differ accordingly, and the cases referred to as "stronger" and "weaker" are relative to each other, rather than against the absolute thresholds in section 2.3.1. For the stronger grid simulated, I_{sc} was set to 30 kA, and for a weaker grid, the same current was set to 10 kA. Assuming an X/R-ratio of 10 and calculating the equal grid impedance based on (2.6), the equivalent grid resistance and inductance are calculated as

$$R_{grid} = \frac{Z_{grid}}{\sqrt{1 + \frac{X}{R}^2}} \tag{3.1}$$

$$L_{grid} = \frac{R_{grid} * \frac{X}{R}}{2 * \pi * f_{grid}} \tag{3.2}$$

, where f_{grid} is the power system frequency of 50 Hz. The grid resistance- and inductances are presented in Table 3.2.

Table 3.2: The two grid strengths considered and calculated grid resistance- and inductances.

Grid strength [kA]	Grid resistance R_{grid} [Ω]	Grid inductance L_{grid} [H]
Stronger, I_{sc} = 30	0.4213	0.0134
Weaker, I_{sc} = 10	1.2639	0.0402

To generate harmonics using the harmonic generator, the voltage source is set to a base frequency of n*f_0, where n is the order of harmonic introduced and f_0 is the fundamental frequency of 50 Hz. The resistance in series with the harmonic generator is used to dampen the magnitude of the inserted harmonic with the size n*100 Ω.

The two harmonics injected were of the 5th and 9th order. These were chosen, as the most prominent harmonics from the converters are of lower order (as presented in section 2.4.4). The 5th is a negative sequence harmonic, and the 9th is a triplen (a zero sequence), which affects the system response differently compared to other harmonics [40].

3.2.5 Cable energization sequence

To analyze different scenarios of the grid conditions, but still being able differentiate between inherent behavior from the OWPP and the grid and different cases, the simulations were done according to the sequence below, with breaker locations specified in Figure 3.3.

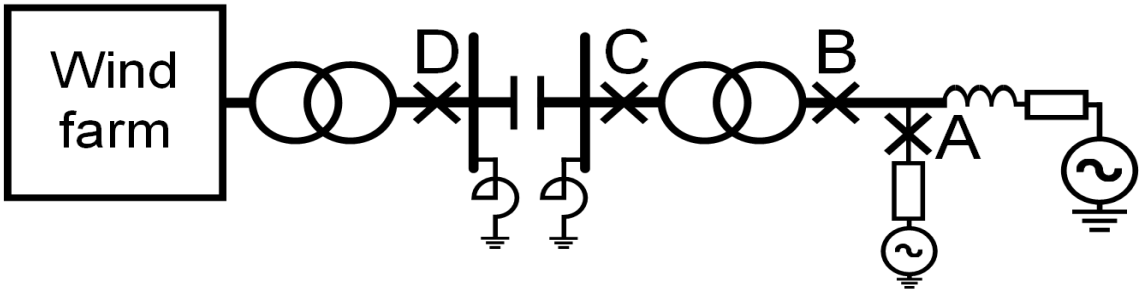

Figure 3.3: Topology of the system with the breaker locations marked as A, B, C and D.

Breaker sequence:

- 0.3 s: Breaker A closes, the harmonic generator is connected.
- 0.5 s: Breaker B closes, the grid is connected to PCC.
- 2.0 s: Breaker C closes, the grid is connected to the export cable.
- 4.0 s: Breaker D closes, the wind farm and the transformer at the OSS are interconnected with the grid.

3.3 Fourier analysis

This section introduces the signal processing methods used to extract harmonic content from the simulated time domain data, and the specific parameter choices made for the analysis in this thesis.

Voltage and current waveforms in a power system are recorded in the time domain, but harmonics are by definition properties visible in the frequency domain. A waveform distorted by harmonics is the sum of a fundamental sinusoid (50 Hz in this work) and additional sinusoids at integer multiples of that fundamental: 100 Hz, 150 Hz and so on. To quantify how much of each harmonic is present in a measured signal, the signal must be decomposed into its frequency components. This decomposition is performed using the Fourier transform [80].

The Fast Fourier Transform (FFT) decomposes a sampled time domain signal into the sinusoidal components it contains, presenting the amplitude of each frequency present in the signal [80]. It is the standard tool for harmonic analysis in power systems, and is the method recommended by IEEE Std 519 for assessing harmonic distortion at the point of common coupling [66]. The principle is illustrated in Figure 3.4, a slightly distorted time domain waveform (Figure3.4(a)) is decomposed into its discrete frequency components (Figure 3.4(b)), where the contribution of each harmonic order can be read directly.

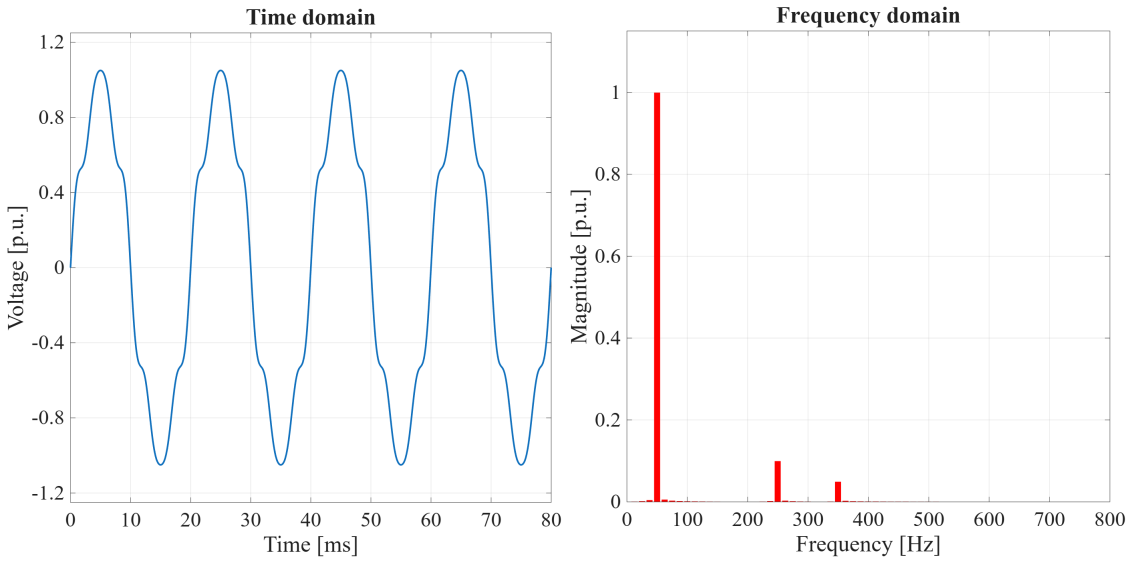

(a) Distorted waveform in the time domain.

(b) The same signal decomposed into its frequency components.

Figure 3.4: Illustration of how the FFT relates time domain waveforms to the frequency domain. The signal contains a 50 Hz fundamental, a 5th harmonic at 10 %, and a 7th harmonic at 5 %.

3.3.1 Sampling rate and the Nyquist criterion

For an FFT to correctly reconstruct a frequency component, the signal must be sampled at a rate of at least double that frequency, according to the Nyquist criterion [80]. If the sampling rate is too low, frequency components above $F_s/2$ are misinterpreted as lower frequencies, and added to the spectrum at the wrong location, a distortion called aliasing. The principle is illustrated in Figures 3.5 and 3.6, where a signal containing a 50 Hz fundamental and a 9th harmonic at 450 Hz is sampled at two different rates. With adequate sampling seen in Figure 3.5, both components appear correctly in the spectrum. With the undersampling in Figure 3.6, the 9th harmonic aliases onto the fundamental, and the spectrum now shows only a 50 Hz component, but its magnitude is inflated and the original 9th harmonic is missing.

In this thesis, the PSCAD plot step of 100 μs corresponds to a sampling frequency of $F_s = 10$ kHz. Frequencies up to 5 kHz can therefore be analyzed without aliasing, which covers the highest harmonic of interest in this work (the 63rd order at 3150 Hz) with sufficient margin.

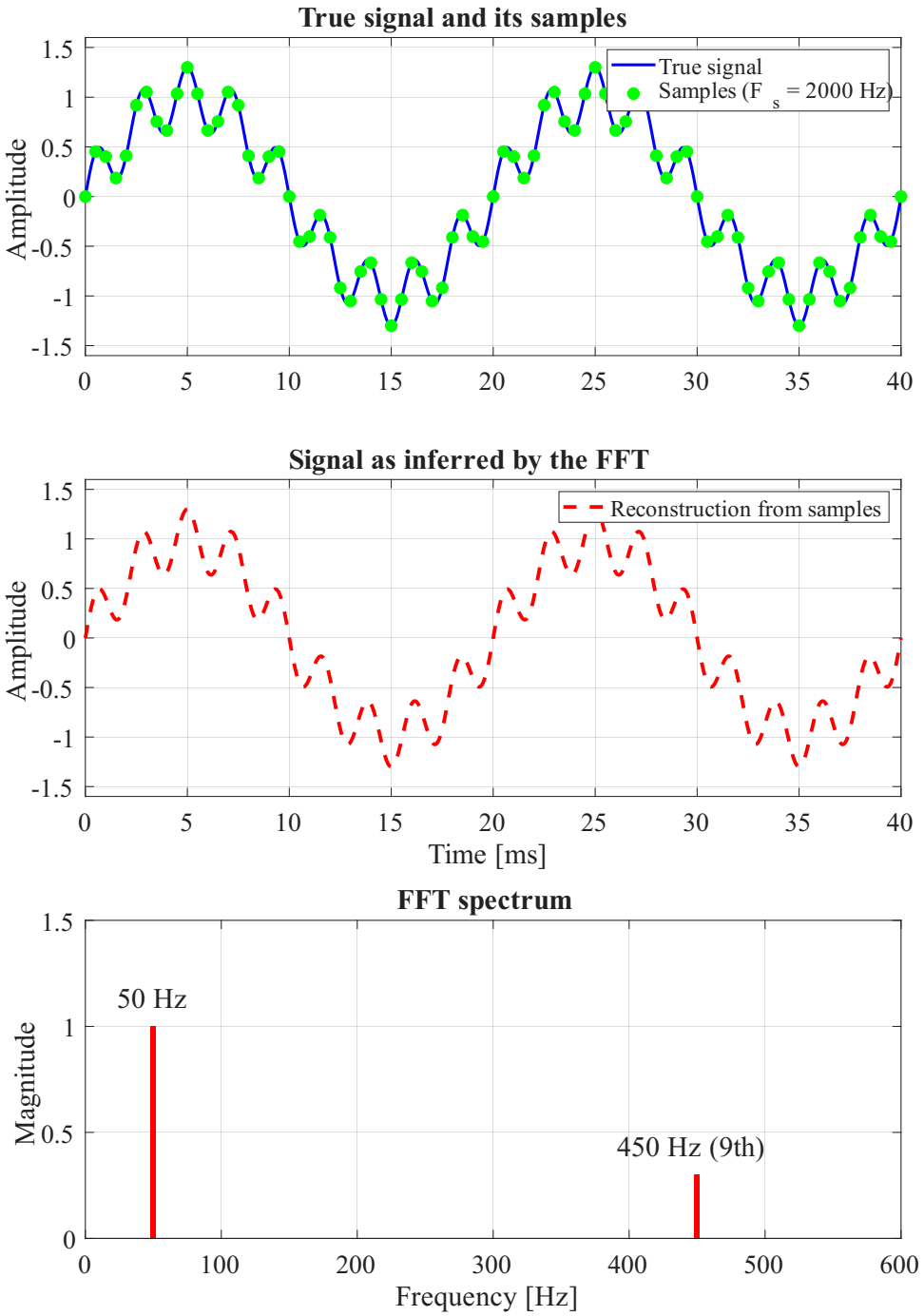

Figure 3.5: Adequate sampling at $F_s = 2000$ Hz. The samples preserve the distorted shape of the true signal, the reconstruction matches the original, and both the 50 Hz fundamental and the 450 Hz 9th harmonic appear in the spectrum.

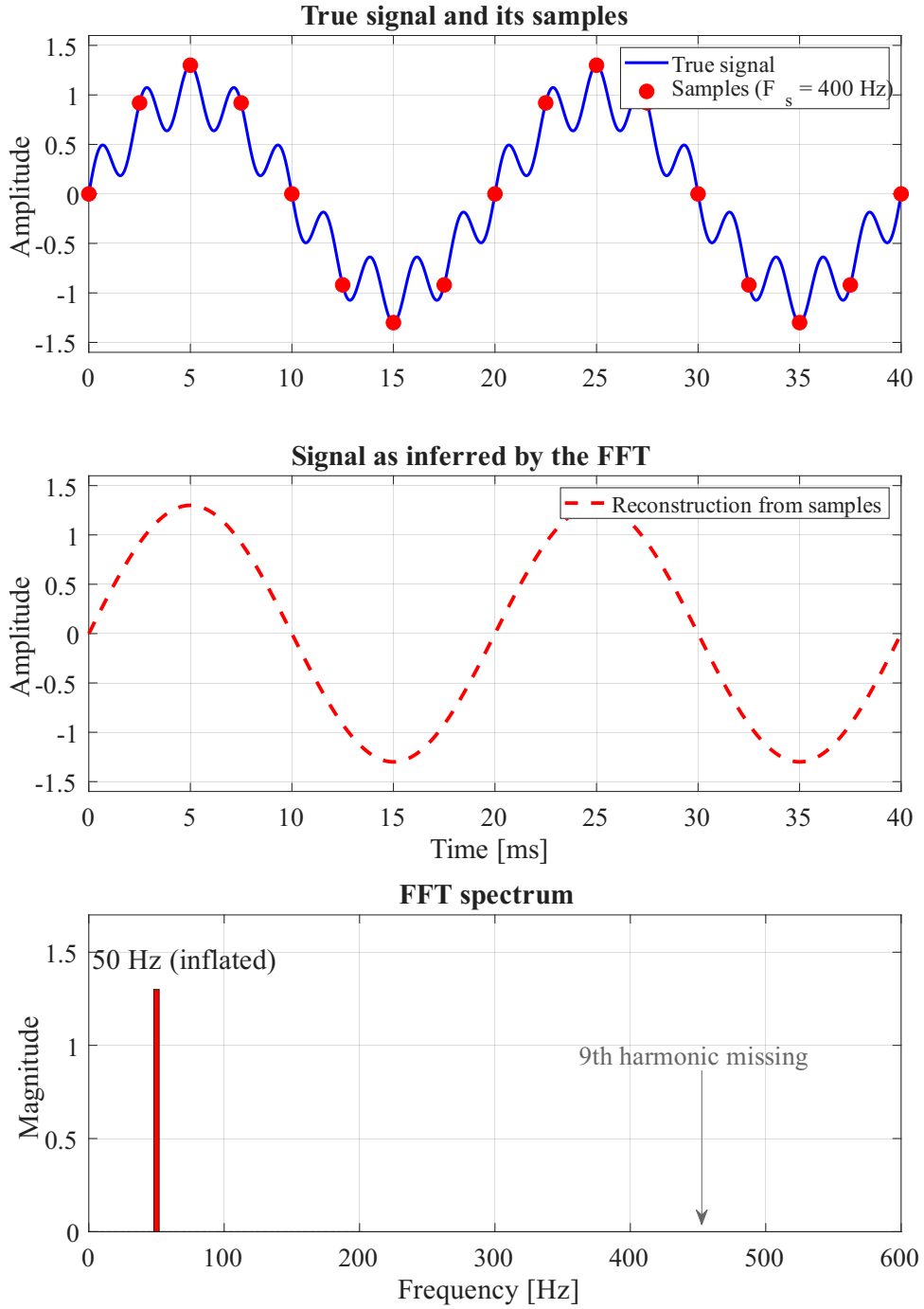

Figure 3.6: Undersampling at $F_s = 400$ Hz. The sparse samples miss the 9th harmonic. The reconstruction is a clean 50 Hz sine, with the 9th harmonic having aliased onto the fundamental (50 Hz) and inflated its magnitude.

3.3.2 Windowing

The FFT operates on a finite block of samples, called a window [80]. A simulation produces several seconds of data, but the FFT is typically applied to a much shorter window. In this thesis, the window length is 80 ms, as it covers four fundamental cycles at 50 Hz. The window is positioned to capture steady-state behavior after the last breaker has closed, from $t = 4.00$ s to $t = 4.08$ s. This selection is shown in Figure 3.7, where the red duration of the signal is the input to the FFT. Choosing the window to span an integer number of fundamental cycles (exactly four in this case) avoids spectral leakage, which would otherwise distort the magnitudes of the harmonic components in the frequency domain.

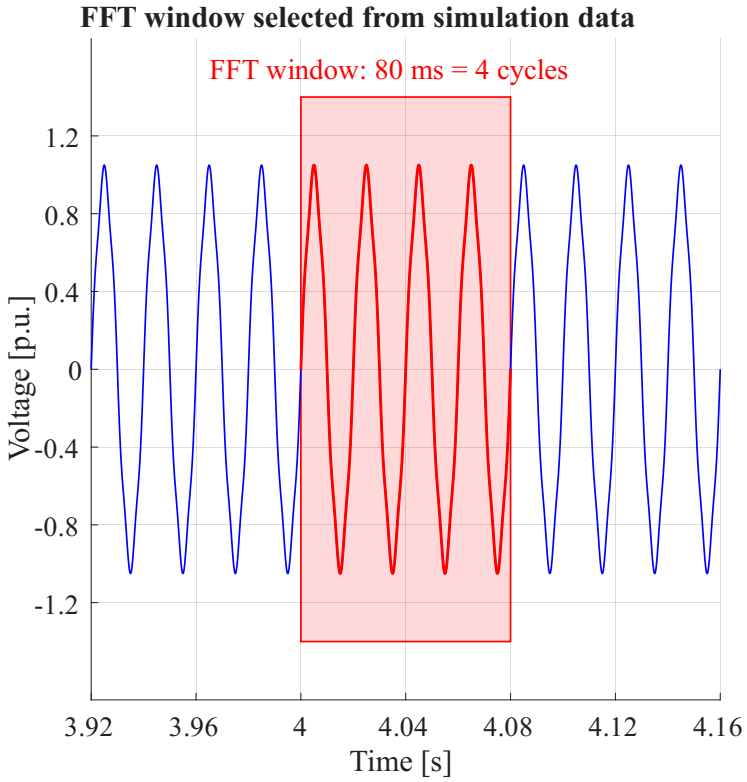

Figure 3.7: The 80 ms FFT window from $t_1 = 4.00$ s to $t_2 = 4.08$ s, covering four fundamental cycles at 50 Hz, used as input to MATLAB's `fft()` function.

3.4 Data gathering and treatment

The PSCAD model runs the simulation for 6 seconds and has a plot step of 100 µs. The voltage, current and phase angles are collected from PSCAD and treated in MATLAB where the signals are subjected to FFT analysis using the sampling rate and window described in section 3.3, and total harmonic distortion (THD) is computed from the resulting FFT.

Two analysis windows are used. The primary window covers 4.00 s to 4.08 s, which is immediately after the last breaker is closed (described in section 3.2.5). This is to ana-

lyze the momentary harmonic distortion when the OWPP is fully commissioned, as the system components are not balanced at this point, and the risk of faults and issues stemming from harmonic distortion is high. To compare the behavior before full energization, a secondary window from 3.46 s to 3.54 s is used to provide a baseline for comparison. Two additional windows are used in section 5.6.3 as a sensitivity check and ensure that the THD values are not the result of a single window choice.

The voltage ratio presented is in percentage of the fundamental frequency, with the harmonic order (up till the 63rd) along the x-axis. The harmonic impedance is calculated using (2.13), (2.14) and (2.15), and is presented in real and imaginary parts in Ohms, with the harmonic order along the x-axis.

3.5 Hypothesis

Based on the theory in section 2, the following is to be expected from the simulations:

Cable length and resonance: The system resonance frequency f_{res} is inversely proportional to $\sqrt{LC}$ as seen in equation 2.3. Longer cables have a greater shunt capacitance, which shifts resonances to lower harmonic orders. Because of this, longer cables are expected to amplify lower order harmonics more than shorter cables. At frequencies above resonance, the shunt capacitance works as a low-impedance path to ground, as X_C decreases with frequency according to equation 2.2, which is expected to attenuate higher order harmonics.

Grid strength and harmonic distortion: Weaker grids (lower SCR) provide less damping capabilities and result in a greater THD at PCC, in comparison to stronger grids, as mentioned in section 2.3.1.

Order of injected harmonic: A 9th order injection is anticipated to be more attenuated than a 5th, as the dampening resistance in the harmonic generator scales with n due to n*100 ohm. The 9th order is also chosen as a triplen (zero sequence) representative to contrast with the 5th order (negative sequence), and observe how harmonics of different sequence types interact with the system.

4
Results

In this section, the results from the simulations are presented in the voltage and impedance domain respectively. They both go through the cases of strong and weak grids, when using a longer and shorter cable and when injecting a 5th and 9th order voltage harmonic respectively. At the beginning of both subsections, the behavior before full system energization in respective domain is presented.

4.1 Voltage harmonics data

In this section, the voltage harmonics for strong and weak grids and long and short cables when injecting a 5th and 9th order harmonic are presented. There is a comparison between the cases in section 5.3.

4.1.1 Phase to ground voltage in the time domain

In Figure 4.1(a), the voltage harmonics for a stronger grid with a great 5th and 9th order harmonic injected from the grid using a 100 km cable is presented. It shows how phase voltage varies over time, and that voltage vastly varies around the switching events, before reaching steady-state.

In Figure 4.1(b), the harmonics for a smaller interval are shown. It displays how the sine wave becomes significantly more distorted when the system is fully energized at 4 seconds. As previously mentioned, the calculations and data presented below are based on the last switching event, where the entire system becomes energized at 4.00 s.

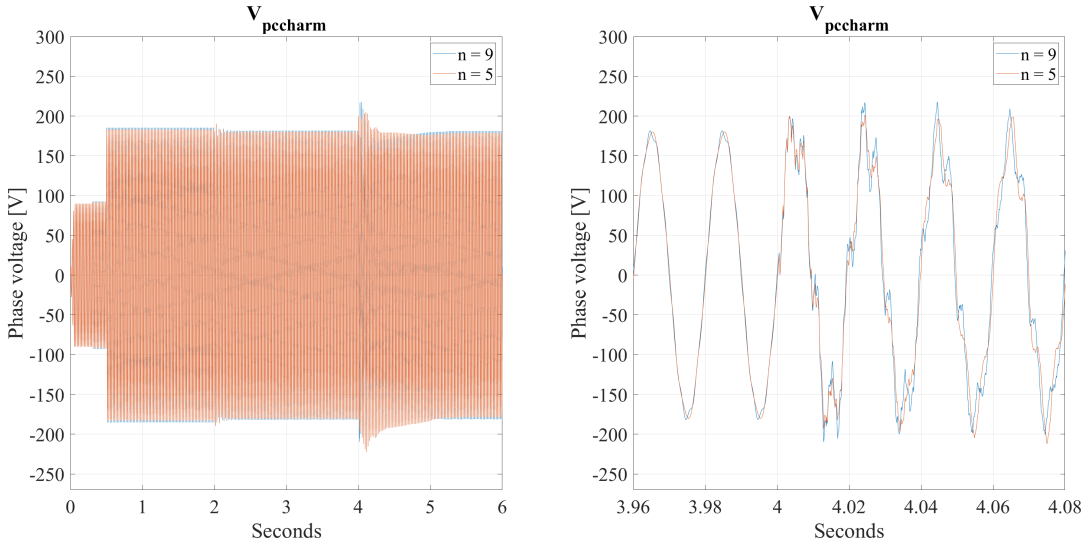

(a) 100 km cable phase voltage in time domain.

(b) 100 km cable zoomed in at 4.01 seconds.

Figure 4.1: Phase voltage in the time domain. Stronger grid, 100 km cable, injected 5th order harmonic.

4.1.2 Voltage behavior before full cable energization at 3.5s

In Figure 4.2(a), the voltage in the frequency domain is presented. It demonstrates that the harmonics at this point in time are close to zero, except for the injected 5th and 9th harmonics respectively. This indicates that the harmonic generator is working, and that the grid side of the system does not inherently have any great voltage harmonics. Both injected harmonics are of roughly the same magnitude, with the 9th being slightly greater. Figure 4.2(b) is zoomed in on the 20 first orders.

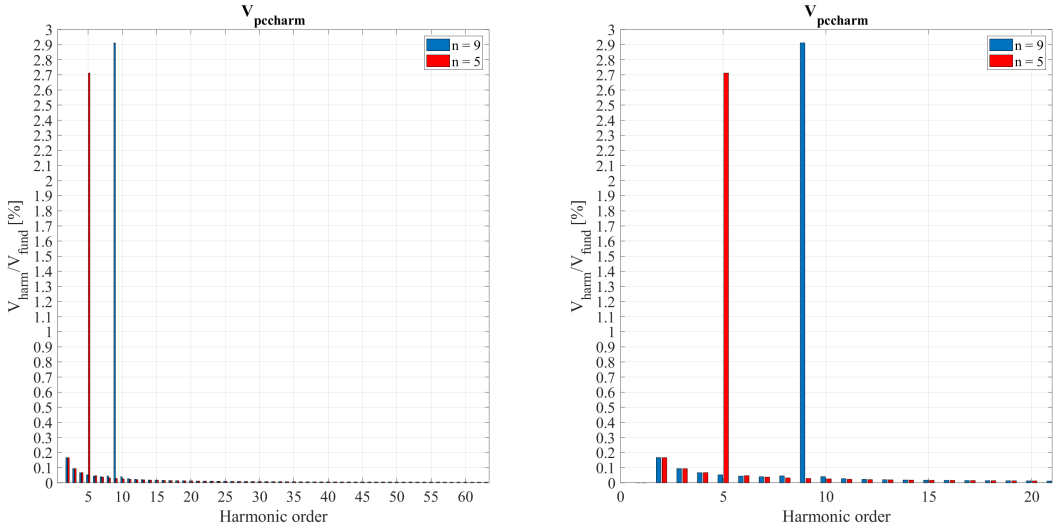

(a) 100 km cable phase voltage harmonics at 3.5 seconds.

(b) 100 km cable zoomed in at 3.5 seconds.

Figure 4.2: Voltage in the frequency domain for a stronger grid with injected 5th & 9th order voltage harmonics.

4.1.3 Voltage total harmonic distortion

Presented in Table 4.1 are the voltage total harmonic distortions (THD_v) for different cases. When injecting a 5th order harmonic, the harmonic distortion was always greater for shorter cables, no matter if the main grid was stronger or weaker. However, when injecting a 9th order harmonic into a stronger grid, the THD was the greatest for the longest cable (100 km), but when injecting into a weak grid, the THD was the greatest for the shorter cable (50 km). Overall, the THD is greater for weaker grids compared to stronger grids.

Table 4.1: THD_v for different injected harmonics and for stronger and weaker grids with 100 and 50 km cables respectively.

Case / Injected harmonic	Strong 100 km	Strong 50 km	Weak 100 km	Weak 50 km
n = 5	9.10 %	10.38 %	37.45 %	40.66 %
n = 9	19.01 %	16.94 %	31.51 %	35.06 %

4.1.4 Case 1: Stronger grid with injected 5th & 9th order voltage harmonics

100 km cable (see Figure 4.3(a)): The harmonic of greatest magnitude ($\backsim$18 %) is found at the 5th order when injecting a 9th order harmonic. The second greatest magnitude ($\backsim$7 %) is found at the same order, but when injecting a 5th order harmonic. Local peaks

(in descending order of magnitude) appear on the 20th, 56th, and 38th orders.

For both injections, the spectrum is dominated by the listed peaks, with all other harmonic orders being below 1 %. The 5th order stands out as the dominant harmonic, regardless of which order is injected, suggests that the system has a resonance near the 5th order that any injected harmonic ends up exciting.

50 km cable (see Figure 4.3(b)): A similar behavior is found as for the 100 km cable, but the magnitudes are slightly lower for the 5th order harmonic when injecting a 9th ($\backsim$16 %) and 5th ($\backsim$9 %) order harmonic respectively. This is indicating that cable length does not significantly shift the resonance for strong grid conditions.

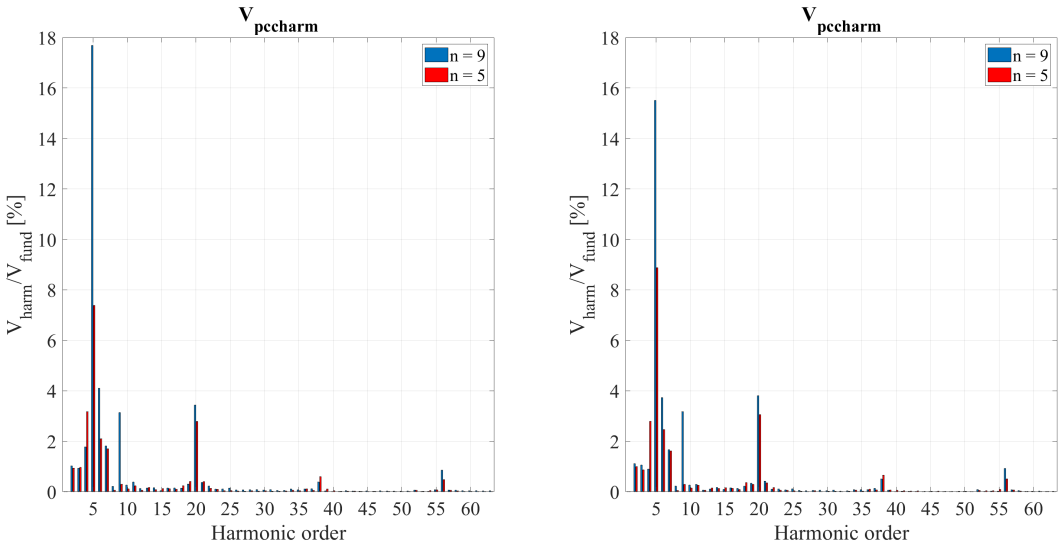

(a) 100 km cable.

(b) 50 km cable.

Figure 4.3: Voltage harmonics at 4.01 s for a stronger grid with injected 5th & 9th order harmonics.

4.1.5 Case 2: Weaker grid with injected 5th & 9th order voltage harmonics

100 km cable (see Figure 4.4(a)): The harmonic of greatest magnitude ($\backsim$36 %) is found at the 4th order when injecting a 5th order harmonic. The second greatest magnitude ($\backsim$29 %) is also found at the 4th order, but when injecting a 9th order harmonic. After the dominant 4th order, additional local peaks appear (in descending order of magnitude) at the 5th, 3rd, 2nd, 19th, 20th, 37th, 38th, and 56th orders. Outside these local peaks, both injections show negligible harmonic content above the 9th order (<1 %).

When the 5th order is injected, the spectrum also shows a noticeable 6th order component, and when the 9th order is injected, the 9th order component itself stands out (the injected harmonic). Compared to the stronger grid case, the dominant harmonic has shifted from the 5th order down to the 4th, and the magnitudes are roughly four times higher. This is

consistent with a weaker grid lowering the resonance frequency, and providing less damping.

50 km cable (see Figure 4.4(b)): A similar behavior is found as for the 100 km cable, but the magnitudes are instead slightly greater for the 4th order when injecting a 5th (⌣39 %) and 9th (⌣31 %) order harmonic respectively. This is the opposite to what was seen in the strong grid case, suggesting that the longer cable contributes some additional damping when the grid is weak.

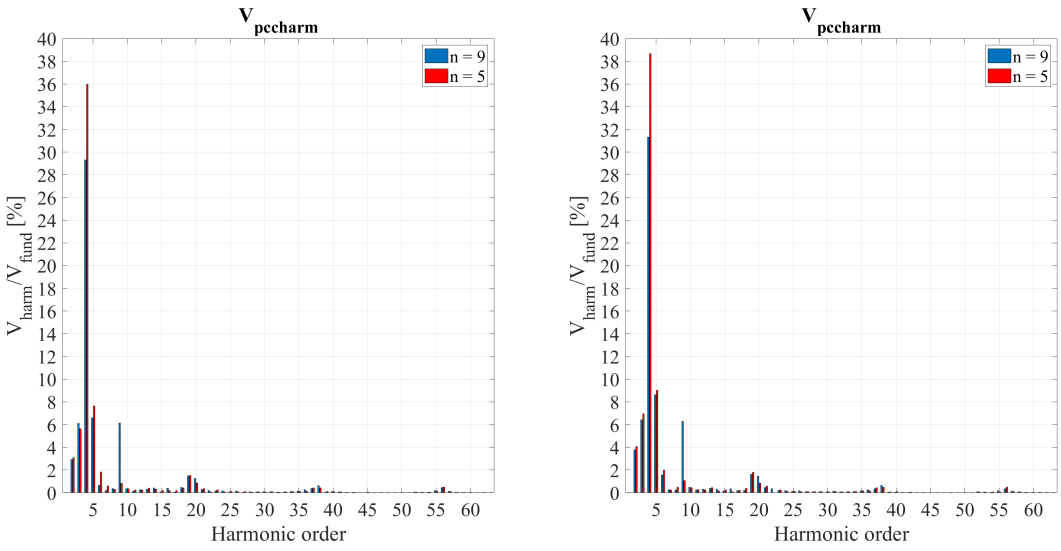

(a) 100 km cable.

(b) 50 km cable.

Figure 4.4: Voltage harmonics at 4.01 s for a weaker grid with injected 5th & 9th order harmonics.

4.2 Harmonic impedances data

Harmonic impedance follows Ohm's law no matter what frequency it is. Even at higher frequencies like 3 kHz, a low harmonic impedance at PCC means that a harmonic voltage source drives a correspondingly large current. Low harmonic impedance at the PCC hence correlates to poor harmonic performance, as it allows for large harmonic currents to flow into the grid. Examining the impedance across the harmonic spectrum gives a complementary perspective to the voltage analysis in section 4.1, and an understanding of where the system is most susceptible to harmonic amplification.

The voltage results in section 4.1 show what the harmonic distortion looks like at the PCC for each case. The harmonic impedance presented in this section shows why. It identifies the frequencies at which the system is susceptible to amplifying any harmonic current that happens to be injected. The two perspectives give a complementary view, where voltage shows the outcome, and impedance shows the mechanism behind it.

4.2.1 Harmonic behavior before full cable energization at 3.5s

In Figure 4.5(a), the resistive impedance in the frequency domain is presented. It shows that the resistive harmonic impedance at this point in time varies a lot depending on the harmonic order, with the 9th order injection being significantly greater for most orders than the 5th order injection. The greatest magnitude is found at the 3rd order when injecting a 9th order harmonic and is roughly 2200 Ω. For the 5th order injection, the greatest harmonic is found at the 10th order and is at 550 Ω.

Figure 4.5(b) shows the reactive impedance at the same point in time. This time, the two injection cases are not as varied in magnitude when comparing between the 5th and 9th order injection. The 9th order injection is still the greatest though, with the greatest magnitude being found at the 3rd order and is roughly 9.5 Ω. For the 5th order injection, the greatest magnitude is found at the 10th order and is roughly 4 Ω.

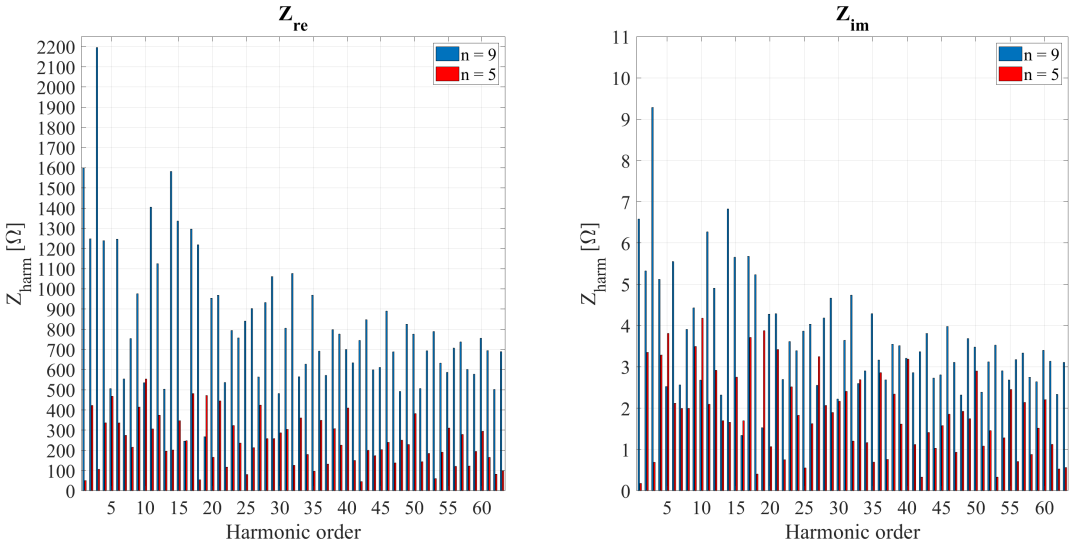

(a) Z_{re} harmonics.

(b) Z_{im} harmonics.

Figure 4.5: Resistive and reactive components of the impedance for the stronger grid case with a 100 km cable before full system energization.

The reactive part was inspected for all eight simulated cases by plotting the imaginary part across all 63 harmonic orders. In every case, Z_{im} remained positive (inductive), so the reactive plots are not reproduced for each case. A complete analysis of the reactive component across all cases is left for future work.

4.2.2 Case 1: Stronger grid with injected 5th & 9th order voltage harmonics

100 km cable: The resistive impedance is scattered as seen Figure 4.6(a), and there is no pattern to be found. The greatest magnitude when injecting a 5th order harmonic is roughly 360 Ω at the 3rd order, and roughly 440 Ω at the 2nd when injecting a 9th order harmonic. When injecting a 5th order harmonic component, the greatest magnitudes

are found at the 3rd, 17th and 14th orders. When injecting a 9th order harmonic, the greatest magnitudes are found at the 2nd, 44th and 15th orders. For most orders, the 9th order injection cases result in harmonics of greater magnitude than the 5th order injection.

The lack of a clear pattern in the resistive impedance under a strong grid reflects the grid's stiffness. The impedance seen from the PCC is dominated by the cable and the transformer, rather than the grid itself, and resonance peaks are correspondingly small.

50 km cable: The resistive impedance shown in Figure 4.6(b) displays an intermittent pattern when injecting a 9th order harmonic, where there are groups of higher magnitudes around the 2nd, 9th, 18th, 28th, 36th, 48th and 56th orders. All of these are close to multiples of the injected harmonic. For the case of a 5th order injection, there is not a clear pattern to be found. The greatest magnitude when injecting a 5th order harmonic is found at the 18th order of roughly 370 Ω, and the greatest magnitude when injecting a 9th order harmonic is found at the 37th order at roughly 930 Ω. The intermittent grouping suggests that the shorter cable amplifies the injection frequency and its multiples more than other frequencies.

Compared to the 100 km cable, the greatest magnitudes when injecting a 5th order harmonic are roughly the same, while the greatest magnitudes when injecting a 9th order harmonic are doubled when using a 50 km cable.

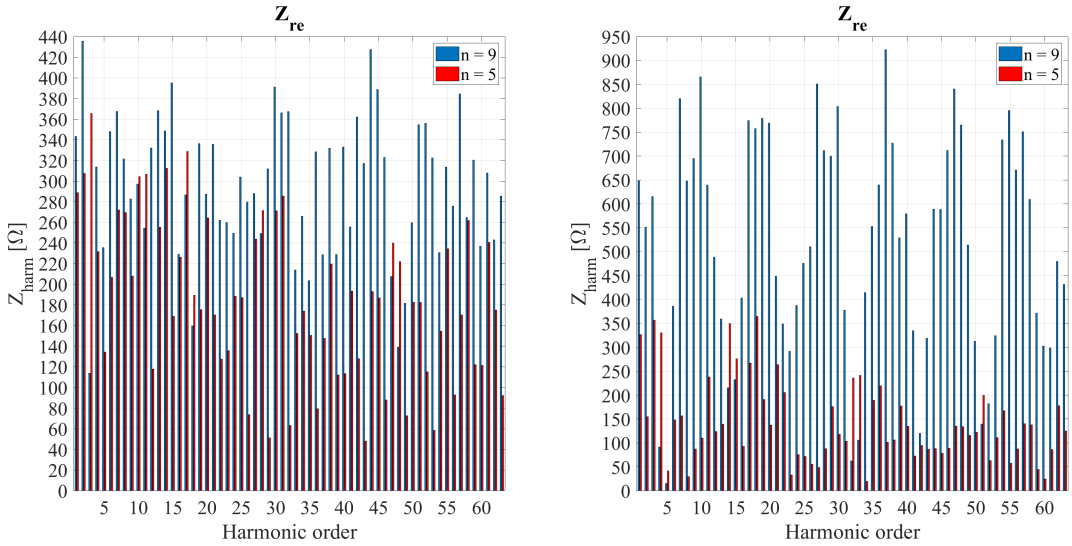

(a) 100 km cable.

(b) 50 km cable.

Figure 4.6: Resistive component of the harmonic impedance for a stronger grid with injected 5th & 9th order harmonics.

4.2.3 Case 2: Weaker grid with injected 5th & 9th order voltage harmonics

100 km cable: The resistive impedance presented in Figure 4.7(a) shows that when injecting a 9th order harmonic, the magnitude of each order is decreasing on average up till roughly the 56th order, where it increases again. The 5th order injection has a more random pattern, but it could be resembling a dampened sine wave. The greatest magnitude when injecting a 5th order harmonic is found at the 5th order with an impedance of roughly 1100 Ω and when injecting a 9th order harmonic, the highest magnitude is found at the 2nd order of roughly 650 Ω.

This decaying magnitude with increasing harmonic order, particularly noticeable for the 9th order injection, indicates that the weaker grid combined with the longer cable presents the highest impedance at low orders. This aligns with the voltage results, where lower order harmonics dominate across the spectrum.

50 km cable: The resistive impedance in Figure 4.7(b) displays a random pattern for both the injection of a 5th and 9th order harmonic. The greatest magnitude when injecting a 5th order harmonic is found at the 5th order and is at roughly 330 Ω, while greatest magnitude when injecting a 9th order harmonic is found at the 3rd order at roughly 130 Ω. There is no indication of the magnitudes decaying for higher orders, but it can be noted that the greatest magnitudes are found for lower orders for both injection cases.

Comparing the 100 km to the 50 km cable, the longer one displays harmonics of greater magnitude overall, and most harmonics are over 200 Ω for the longer cable. The lower impedance magnitudes for the shorter cable do not translate into lower voltage distortion in the corresponding case in section 4.1, where the shorter cable produced a higher THD.

This is because the voltage for each harmonic depends on both the impedance and the harmonic current flowing through it. A small impedance can still produce a large voltage drop if the current is large enough. The impedance plot itself is therefore not sufficient to predict the voltage distortion, as the two perspectives need to be combined, with the impedance pointing to which frequencies are susceptible to amplification, and the voltage results showing the resulting distortion at the PCC.

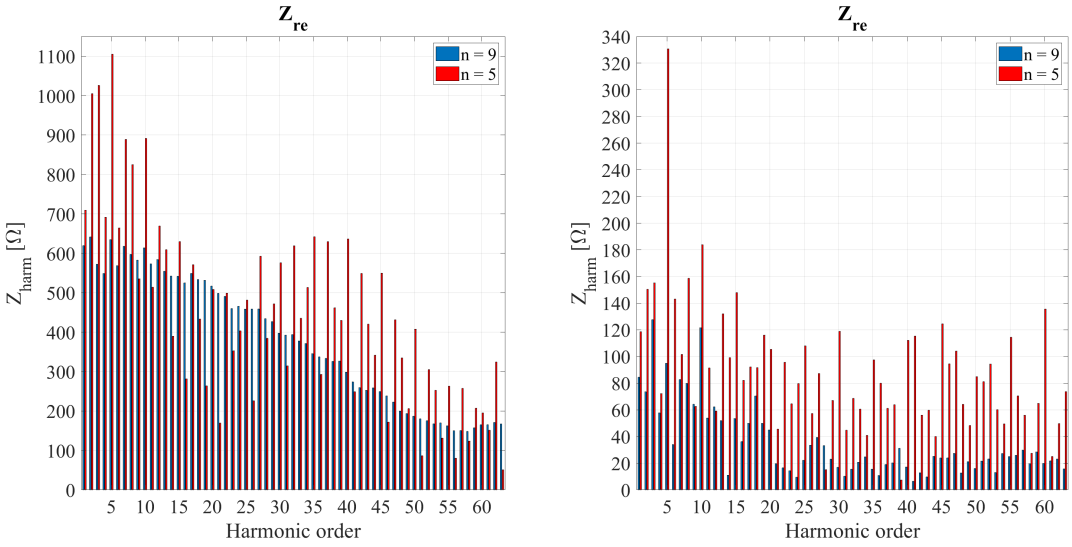

(a) 100 km cable.

(b) 50 km cable

Figure 4.7: Resistive component of the harmonic impedance for a weaker grid with injected 5th & 9th order harmonics.

5
Discussion

In this section, the analysis of the results in the voltage and impedance domain are presented respectively. It also goes over some drawbacks of the way the simulations were conducted, and suggests things to improve for future analysis.

5.1 Key findings summarized

The thesis investigates three main questions regarding harmonic distortion generated by OWPPs. The simulations provided answers to the questions:

Impact of cable length and harmonics at PCC:
The effect of cable length on THD depends a lot on the grid strength. For weaker grids, shorter cables always gave a higher THD, by 8.6 % and 11.3 % for the 5th and 9th order injections respectively. For stronger grids, the result depended on which harmonic was injected: a 5th order injection still gave a higher THD with the shorter cable (by 14.1 %), but for a 9th order injection, the shorter cable actually reduced THD by 10.9 %.

This suggests that the additional shunt capacitance of a longer cable does not act in isolation: the inductance is also increased with length, and the resulting resonance behavior depends on both the grid impedance and the order of the injected harmonic.

Impact of grid strength on harmonics at PCC:
Grid strength is the dominant factor affecting harmonic distortion in the post-energization transient. Weaker grids consistently showed a THD 2-4 times greater than stronger grids for all cases. For example, with a 100 km cable and a 5th order harmonic injection, the THD increased from 9.1 % (stronger grid) to 37.5 % (weaker grid). This highlights the importance of a stronger grid for OWPP integration.

Impact of the order of the injected harmonic:
The observed behavior varied significantly between 5th and 9th order harmonic injections. In stronger grids, 9th order harmonic injection produced a higher THD (19.01 %) than 5th order injection (9.1 %). For weaker grids the relationship reverses: 5th order injection produced higher THD (37.45 %) than 9th order (31.51 %).

This reversal suggests that the position of the system's resonance peak relative to the injected frequency determines the amplification. For stronger grids, the resonance lies near the 5th order, while in weaker grids it shifts toward the 4th. A 5th order injection therefore

drives the resonance more strongly in the weaker grid case, while in the stronger grid case the 9th order injection still excites the 5th order resonance through the system's harmonic interaction, producing a 5th order voltage harmonic of significant magnitude as seen in Figure 4.3. Confirming this would require identifying the resonance peaks in each case, which is suggested for future studies.

5.2 Theoretical implications and model behavior

The simulation results deviate from the hypothesis stated in section 3.5 on several points, which gives insight into both the model limitations and the system behavior.

Grid strength and cable length hypotheses: The hypothesis on grid strength, that weaker grids would produce greater THD due to less damping, is supported by the results. The simulated weaker grid produced a THD 2-4 times higher than the stronger grid for all casees. The hypothesis on cable length, that longer cables would amplify lower order harmonics more by shifting the resonances down, only partly lines up with the results. A shift towards lower orders can be seen when comparing the strong grid (5th order dominant) to the weaker grid (4th order dominant), but the shift comes from the grid strength rather than the cable length, and the THD is not always higher for longer cables.

Injected harmonic order hypothesis: The hypothesis on injected harmonic order, that the 9th order injection would be more attenuated than the 5th, is disproved in the strong grid case, where the 9th order injection produced a higher THD (19.01 %) than the 5th (9.10 %). In the weaker grid case, the relationship instead aligns with the hypothesis, with the 5th order injection producing a higher THD than the 9th. This reversal is explained by the position of the system resonance relative to the injection frequency, which is discussed below.

Absence of characteristic converter harmonics: The theoretical behavior with consistent harmonics occurring around $f_{gc} \pm 2f_e$ (approximately 38th and 42nd orders for a 2 kHz switching frequency) could not be observed in the simulation results. The reason is likely that the aggregated OWPP model does not simulate the actual switching mechanism of the converters. This limitation means that the simulations cannot assess if converter generated harmonics or grid-side harmonics play a bigger role.

Lower order harmonic dominance: The simulations display significant harmonics below the 9th order, with prominent harmonics around the 4th and 5th orders. This means that while the model is not capable of capturing the converter switching harmonics, it displays the lower order resonances that originate from the interactions between grid impedance and the cable impedance.

Resonance behavior: The expected shift in the dominant harmonic order for longer cables, expected from equation 2.3, could not be clearly observed. Instead, a shift is observed from a 5th to a 4th order dominance when comparing a stronger to a weaker grid. This suggests that the grid strength has a larger impact on resonance frequency rather than

cable length.

5th order dominance: The characteristic converter harmonics (5th and 7th orders) that theory predicts are not consistently dominant in the results, except for the 5th order, which does appear prominently, but likely amplified by the injected 5th order harmonic from the grid rather than originating from the BTB-converter itself. The 5th order remains dominant even when a 9th order harmonic is injected, which suggests that the system has a resonance near the 5th order, which any injected harmonic ends up exciting.

Unexplained excitation mechanism: The exact mechanism by which a 9th order injection excites a 5th order resonance more strongly than a direct 5th order injection is not fully explained by the linear interaction between cable capacitance and grid inductance, and is suggested as a topic for future studies, as also stated in section 5.7.

The hypotheses from section 3.5 are not fully matched by the results. The grid strength hypothesis is supported by the results, but the cable length and harmonic order hypotheses do not match in all cases. There are two modeling choices that may have contributed to this. The first is that the aggregated wind farm model does not reproduce the converter switching events, which means that the characteristic switching harmonics around $f_{gc} \pm 2f_e$ are missing from the results. The second is that the shunt reactor sizing was tuned for unity power factor at the fundamental frequency, which does not necessarily reduce harmonics at other frequencies, and could partly hide the expected resonance shift that comes with increasing cable length.

5.3 Analysis of voltage results

Comparison before and after energization: Comparing the voltage harmonics before energization (Figure 4.2) with the other voltage figures during energization, it is apparent that the high magnitude harmonics were not present in the system before full energization, where the system was comprised of the main grid, harmonic generator and onshore transformer. This means that the connection of the offshore transformer and OWPP induces harmonic currents into a network whose resonance behavior amplifies them, resulting in distortion at the PCC.

Before energization, harmonics remain below 0.2 %, decaying steadily with increasing harmonic order (excluding the injected 5th and 9th order harmonics). This confirms that the observed distortion comes from the interaction between the OWPP and grid, rather than pre-existing grid harmonics.

Harmonic magnitude patterns in stronger vs weaker grids: The greatest magnitudes are found in the cases with weaker grids, and the greatest harmonics are within ($\pm$1) order of the same harmonic, no matter if the grid is weaker or stronger. The difference is that for strong grids, harmonics of great magnitude are found at the 5th and 20th orders, while for weaker grids, these are found at the 4th and 19th orders instead. Comparing the 20th, 38th and 56th order harmonics in the stronger grids with the weaker grids, it can be

concluded that the harmonics are noticeably attenuated for weaker grids, indicating that weaker grids dampen higher-frequency components.

Impact of injected harmonic order: In the stronger grid case, the 9th injected harmonic is mostly of greater magnitude compared to when injecting a 5th order harmonic, with the exception of the 36th order. The reversed is observed when looking at the weaker grid, the 5th order injected harmonic is most often of greater magnitude compared to when injecting a 9th order harmonic. This reversal demonstrates grid strength significantly impacts the interaction between injected harmonics and observed harmonics.

Cable length effects: For stronger grids, the magnitude of the harmonics is very similar, with the exception of the 5th order harmonic, which is attenuated for shorter cables compared to longer. For weaker grids, the harmonics are noticeably amplified for shorter cables.

Harmonic distribution patterns: There is no clear cyclic pattern regarding which orders the harmonic peaks are visible, but the majority of the peaks concentrate on low orders (4-5), followed by a smaller group around the 19-20th orders. The 38th and 56th order peaks are less than 1 %, and can be considered negligible. The 9th order peak, when present, likely originates from the 9th order injection, as it is not of noticeable magnitude when injecting a 5th order harmonic.

The voltage THD in weaker grids was greater when using shorter cables compared to longer, for both injections. This behavior was also seen when injecting a 5th order harmonic into a stronger grid, but when injecting a 9th order harmonic, the THD was instead greater for a longer cable. This may be because the shunt reactor sizing was tuned for a power factor close to unity at the fundamental frequency, which does not necessarily reduce harmonic distortion at other frequencies.

5.4 Analysis of harmonic impedance results

While the voltage analysis in section 4.1 shows the resulting distortion at the PCC, the harmonic impedance shows where the system is susceptible to amplifying any harmonic current that gets injected. According to Ohm's law, the harmonic voltage at a given order is the product of the harmonic current and the harmonic impedance at that frequency. This means that peaks of the resistive impedance correspond to frequencies where even modest harmonic currents can drive significant voltage distortion.

Comparing harmonic behavior before and during full system energization: For all cases when injecting a 9th order harmonic, the resistive part displays the greatest peaks before energization. This is not necessarily the case when injecting a 5th order harmonic, depending on the harmonic order. Once the export cable and OWPP are connected, the resistive peaks shift, which aligns with what equation 2.3 predicts: adding the cable changes both L and C, and the resonance frequency $f_{res} = 1/(2\pi LC)$ changes accordingly.

Resistive impedance patterns: Comparing the longer cable with the shorter, the resistive part displays a more random behavior using a longer cable, and a more cyclic behavior for the shorter cable, for the stronger grid case. The cyclic pattern is mostly evident in the case of injecting a 9th order harmonic, and the groups of peaks almost follow the multiples of 9. This suggests that shorter cables create more predictable resonance conditions aligned with the injection frequency and its harmonics, while a longer cable spreads the resonance behavior across more orders. For the weaker grid the relationship is different: the longer cable shows the magnitude decaying with increasing order, while the shorter cable shows a more random pattern.

Lower order dominance for weaker grid: The weaker grid with a 100 km cable in Figure 4.7(a) shows the resistive impedance being highest at lower orders, and decaying for higher orders. This is in line with the weaker grid having a larger inductance, which combined with the cable capacitance, pushes the dominant resonance down to lower orders, where the impedance is therefore highest. This explains why the same case has the greatest THD in the voltage results, with the dominant harmonic shifted from the 5th to the 4th order compared to the stronger grid case.

Magnitude relationships: Resistive impedances are in the magnitude of hundreds of ohms, while the reactive impedances remain at a magnitude of tens of ohms. As the reactance is strictly positive, this indicates that the inductive parts are dominating for all harmonic orders.

Grid strength correlation: For stronger grids, shorter cables produced greater harmonic impedance magnitudes. This relationship was inverted for weaker grids, where instead longer cables resulted in greater impedances. This is consistent with the THD patterns seen earlier, and shows that both grid strength and cable length need to be considered when designing the system.

Negative resistance behavior: No negative resistive harmonic impedance is displayed. As the negative-resistance behavior described in 2.4.11 originates from the converter control of the GSC, this is consistent with the aggregated wind farm representation, which does not capture the converter switching events as discussed in 5.2 and 5.6. Detecting negative-resistance behavior would require a model that includes how the GSC control behaves at harmonic frequencies.

Voltage and impedance compared: The lower impedance magnitudes for the shorter cable did not lead to a lower voltage distortion in the corresponding voltage results. The voltage at each harmonic depends on both the impedance and the harmonic current flowing through it, which means that a small impedance can still give a large voltage drop if the current is large enough. The impedance plots therefore complement the voltage analysis: the voltage shows the outcome at the PCC, and the impedance points to which frequencies the system is most susceptible to amplification.

5.5 Practical implications for OWPP design & operation

These findings give a few implications for OWPP stakeholders:

Grid strength is the priority: Since grid strength had a much larger effect on THD than cable length, grid strength should be prioritized over cable route optimization when looking to minimize harmonics.

Cable length optimization: For weaker grids, longer cables provided some damping. This is counterintuitive, and suggests that the shortest cable route is not necessarily the optimal one from a power quality perspective.

STATCOM design: For STATCOMs such as those provided by Hitachi Energy, the results suggest that control systems should prioritize compensation of lower order harmonics, and should be able to handle weaker grids.

Comparison of technical solutions: While the simulations focus on a single OWPP topology, the results have implications for choosing between the technical alternatives discussed in section 2.

Filter design: The dominance of lower order harmonics (4th-5th order) suggests that passive filters tuned to these frequencies could be useful, although filters at low frequencies tend to be physically large. Passive filters also have a fixed tuning, which makes them less suitable for the varying grid conditions an OWPP may be subjected to [64], [65]. Active filters, including STATCOMs, can handle changing harmonics and varying grid strength [65], [81], which the results indicate can shift the dominant harmonic from the 5th to the 4th order. The absence of significant higher order harmonics in the simulations is partly a consequence of the aggregated wind farm model, which does not reproduce the converter switching events. Filter design would therefore still need to consider potential switching harmonics from the converter, and may require active filtering to comply with local grid codes.

Reactive power compensation: For reactive power compensation, the comparison narrows depending on need. Shunt reactors are commonly used for compensating the capacitive reactive power produced by long submarine cables, and were used in this thesis [15], [16]. They are passive and appropriate for fixed compensation, but cannot adjust dynamically to varying grid conditions. Capacitor banks and SVCs give faster compensation, but are limited in resolution and can introduce additional harmonics [69]. STATCOMs provide continuous and fast compensation at higher cost and complexity [69], with the added benefit that they can also provide active filtering [81].

Converter type: For converter type, the high harmonic distortion levels observed in the weaker grid cases strengthen the case for grid-forming converters over grid-following ones in such conditions, as GFM converters provide voltage support and behave more favorably in low SCR conditions [23], [46], as mentioned in section 2.1.4. The simulations in this thesis used GFL converters, so the results most directly apply to GFL-based

OWPPs.

Transmission technology: Despite the fact that this thesis does not cover the choice between HVAC and HVDC transmission, the trade-off becomes more relevant for longer cables where the cables' reactive power production and resonance behavior have large consequences. The results show that for HVAC, both grid strength and cable length have a significant influence on harmonic behavior at the PCC, which is one of the factors a project would need to consider against the higher cost of HVDC for shorter routes.

Regulatory compliance perspective: All weaker grid cases simulated had THD values in the range of 31-41 % during the post-energization transient, which exceeds the IEEE 519 limit of 1.5 % for high-voltage systems above 161 kV (as mentioned in section 2.4.7) by more than an order of magnitude. While the simulation setup and the aggregated model push these absolute values higher than they would be in practice, and IEEE 519 applies to steady-state operation rather than transients, this large gap shows that harmonic distortion during energization of an OWPP connected to a weak grid could be significant. The sensitivity check in section 5.6.3 shows that THD settles to around 2 % once the system stabilizes, which is closer to the IEEE 519 limit but still above it. Mitigation would be needed, either through grid reinforcement, harmonic filtering, or both, depending on the grid code interpretation.

5.6 Model validation and limitations

Albeit the model did not manage to display all theoretical and hence practical phenomena, the results give valuable input for system design:

5.6.1 Model validity

Three checks support that the model produces results consistent with the established theory and the OWPP harmonics literature.

First, the dominant influence of grid strength on harmonic distortion observed in section 4.1, with weaker grids producing 2-4 times higher THD than stronger grids, is in line with [30], [47], where weaker grid connections are reported to be associated with higher levels of harmonic distortion.

Second, the higher harmonic distortion observed in the weaker grid case is consistent with the higher harmonic impedance presented by the weaker grid Thevenin equivalent. Figure 5.1 shows the magnitude of the grid Thevenin impedance for the two grid strengths used in the simulations across the harmonic spectrum. The weaker grid presents a higher impedance at every harmonic frequency, and by Ohm's law, a higher impedance produces a larger voltage harmonic for the same injected harmonic current. This is the same reason that a 2-4 times higher THD is observed in the weaker grid cases. The downward shift in dominant order from the 5th (stronger grid) to the 4th (weaker grid) is consistent with the

resonance frequency ($f_{res} = 1/(2\pi\sqrt{LC})$) decreasing as the grid inductance L increases for the weaker grid case.

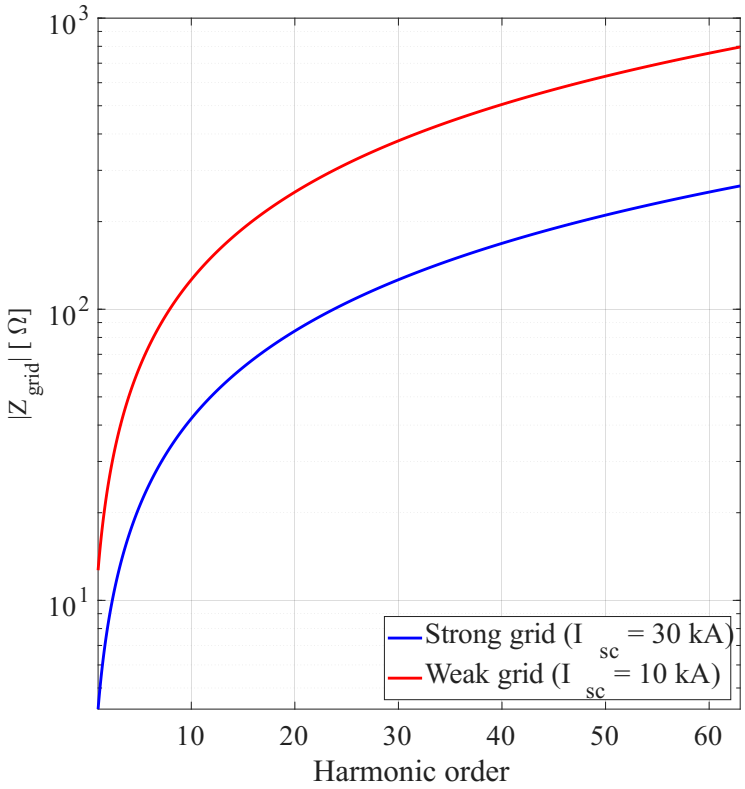

Figure 5.1: Magnitude of the grid Thevenin impedance for the stronger ($I_{sc} = 30$ kA) and weaker ($I_{sc} = 10$ kA) grids used in the simulation, plotted in the frequency domain up to the 63rd order.

Third, the simulated THD ranges (9-19 % for stronger grid, 31-41 % for weaker grid) are consistent with the order of magnitude reported for OWPPs connected to similar grids [13], [30], [47].

The two grid cases are referred to throughout this thesis as ”stronger” and ”weaker” relative to each other, since the SCR was not calculated numerically. Using the definition in section 2.3.1, calculating the SCR would require an explicit choice of S_n, which would tie the conclusions to one specific OWPP size. The relative comparison used in this thesis keeps the findings independent of that choice. Calculating the SCR for a specific OWPP size is suggested as a follow-up in section 5.7.

The two grid cases are referred to throughout this thesis as ”stronger” and ”weaker” relative to each other. The grid strength was set by varying the short-circuit current I_{sc} between 30 kA for the stronger grid, and 10 kA for the weaker grid, and the SCR was not calculated numerically.

5.6.2 Comparison to reported field measurements

The dominance of lower order harmonics observed in the simulations aligns with field measurements reported in the OWPP literature. For example, in [13] it is stated that for large offshore wind farms, the most significant harmonic content tends to be concentrated at lower orders, with lower order resonances arising from the interaction between the cable capacitance and the inductances of the upstream system. This is similar to what is observed in the simulations of this thesis, where the dominant harmonics consistently appeared at the 4th and 5th orders, depending on grid strength. Another example is [30], which states a comparable lower order resonance behavior for OWPPs connected to weaker grids, also consistent with the shift from the 5th order (stronger grid) to the 4th order (weaker grid) found in this work. The qualitative agreement between this finding and previously reported measurements supports the conclusion that the aggregated model captures the system level resonance behavior of OWPPs, even if the absolute THD values are inflated by a deliberately strong harmonic injection, as discussed above.

5.6.3 Model applications and limitations

The aggregated model is therefore appropriate for comparing different grid reinforcement options and cable routes for harmonic studies on a system level. The model is unfortunately not appropriate for converter control, filter dimensioning, and studying switching harmonics from the converters.

Each case was simulated once, and the FFT was applied to a single 80 ms window, right after full energization. The window was selected to capture the immediate post-energization period, since this is when protection systems and equipment are most stressed by harmonic distortion. To verify that the reported THD values are not artifacts of a single window position, additional FFTs were performed at later windows for both the stronger and weaker grid 100 km cases with a 5th order injection. The resulting THD values are presented in Table 5.1, alongside the originally reported values from Table 4.1. Both grid configurations end up at a similar low THD around 2 % as the system settles, meaning that the 2-4 times ratio between weaker and stronger grids reported in this thesis is a property of the immediate post-energization period rather than the steady-state, where the ratio itself also decays as the system settles. This is consistent with the methodology stated in section 3.4, which purposely aims at the post-energization period as the regime of interest. The relative comparisons between cases are still valid since all cases were analyzed using the same window position.

Table 5.1: THD_v at the PCC for different FFT window positions, used to verify that the reported values are not artifacts of a single window choice. Both cases use a 100 km cable with a 5th order harmonic injection.

Window start / Case	$t_1 = 4.00$ **s**	$t_1 = 4.20$ **s**	$t_1 = 5.00$ **s**	$t_1 = 5.50$ **s**
Strong 100 km, n = 5	9.10 %	13.56 %	4.08 %	2.04 %
Weak 100 km, n = 5	37.45 %	33.80 %	9.06 %	1.86 %

The voltage harmonic data presented is in percentage relative to the fundamental frequency. The downside is that if the simulations result in an unlikely scenario, where either the fundamental frequency or the other harmonics are unrealistically proportional to each other, these percentages are irrelevant. It can also obscure scenarios with extremely low or high magnitude harmonics, if all (including the fundamental) are of similar magnitude.

It should also be mentioned that the absolute THD values reported in this thesis are not directly comparable to real grid harmonic levels. The harmonic generator described in section 3.2.4 is a 200 kV source behind only $n \cdot 100\,\Omega$, meaning that the injected harmonic content is significantly higher than the background harmonic levels found on real high voltage transmission systems, where the THD typically remains below 2 % at the relevant voltage levels [53]. The simulations therefore represent a stress-tested injection scenario, designed to show how the system responds when harmonics are present, rather than to predict the harmonic levels at the PCC during normal operation. The relative comparisons between cases (the 2-4 times difference between weaker and stronger grids and so on) are therefore the meaningful results.

5.7 Suggested improvements for future simulations and further analysis

- Improved converter modeling that simulates the switching events of the converters.
- The export cable was modeled using the cable feature in PSCAD, where the line resistance and the reactance per unit length was specified. Instead, the submarine cable feature in PSCAD could be used, where insulation distances, conductor sizes and depth under the seabed can be specified. It is possible this would have given different results, as it would take more factors into account that can affect the harmonic propagation in the cable.
- The inter-array cables were not implemented into the model used. For future simulations, the previously mentioned submarine cable feature could be implemented, but for the lower voltage inter-array cables.
- Variable X/R ratio: It was fixed when running the different cases in order to limit the number of variable factors. Instead I_{sc} was the measure used to control the grid strength. In future simulations, the X/R-ratio could be varied too, or instead.
- The cases used in the simulations do vary the short circuit power, which means that the grid-side is of different strengths. For future simulations, it would be good to

quantify the grid strength in terms of SCR to have concrete results for the defined ”weaker” and ”stronger” grids respectively. This might require model modifications.

- The FFTs were performed by analyzing harmonics during a limited slot in the time-domain, even though the harmonics vary a lot in the time domain. This means that an FFT analysis performed for a different span would have given different results.
- A full analysis of the imaginary part of the harmonic impedance was outside the scope of this thesis. Investigating it in future studies gives a more complete picture of resonance behavior, for example by identifying at which frequencies the system transitions toward resonance peaks, and how this varies with cable length and grid strength.
- It could be interesting to investigate how much the shunt reactors affect the harmonic distortion. Adding breakers for them and analyzing the results before and after the connection of them would give a better understanding of their impact.
- As the injected voltage harmonics were of the 5th (negative sequence) and 9th orders (zero sequence) respectively, it could be interesting to inject a harmonic of a different order, simulating a positive sequence fault.
- An attempt was made to validate the PSCAD model by creating a simplified theoretical impedance model in MATLAB, but the measurements in PSCAD were prevented by the presence of active voltage sources in the system, preventing meaningful comparison. This would be interesting to fully investigate in the future.

6
Conclusion

6.1 Fulfillment of objectives

This thesis investigated the interplay between grid strength, cable lengths, and injected voltage harmonics, and how these affect voltage harmonic distortion and harmonic impedance in OWPPs. The three research questions presented in section 1.3 are revisited below.

How do shorter/longer HVAC cables impact the voltage harmonic distortion and harmonic impedance at the PCC? Cable length effects were smaller than the grid strength effects, but the behavior was complex, and depended on both grid strength and the injected harmonic order. For weaker grids, shorter cables gave higher THD in all cases. For stronger grids, the relationship reversed depending on which harmonic was injected. The harmonic impedance results show the same directional dependence: longer cables gave higher impedance magnitudes in the weaker grid case, but lower magnitudes in the stronger grid case. The finding that longer cables can lower THD in weak grids goes against the intuition that the shortest cable is always best. The shortest route is therefore not necessarily the best one if power quality is considered.

How do stronger/weaker grids impact the voltage harmonic distortion and harmonic impedance at the PCC? Grid strength was the dominant factor in the post-energization transient. Weaker grids gave THD 2-4 times higher than stronger grids for all four cable and injection combinations during the analyzed window, with absolute THD values of 31-41 % for the weaker grid and 9-19 % for the stronger grid. The harmonic impedance results, shown in Figure 5.1, show that the weaker grid has a higher Thevenin impedance at every harmonic frequency, which is the underlying reason for the higher voltage distortion.

The dominant harmonic also shifted from the 5th order in the stronger grid, to the 4th order in the weaker grid. This is consistent with the lower resonance frequency that follows from the larger grid inductance. A sensitivity check on later windows (section 5.6) showed that both grid configurations settle at a similar low THD around 2 % once the system has stabilized. The 2-4 times difference is therefore specific to the post-energization transient, not the steady-state.

How does the order of harmonics injected from the main grid affect the voltage harmonic distortion and harmonic impedance at the PCC? The effect of the injected harmonic order depends on the grid strength. In stronger grids, the 9th order injection produced a higher THD (19.01 %) than the 5th order injection (9.10 %), which is likely because the system has a resonance near the 5th order that any injected harmonic ends up exciting, as discussed in section 5.1. In weaker grids the relationship reversed, with the 5th order injection producing a higher THD (37.45 %) than the 9th (31.51 %), as the resonance had shifted closer to the injection frequency. This shows that the harmonic distortion at the PCC is determined by the position of the system resonance in relation to the injection frequency, not by the injection order alone.

Although the aggregated model does not capture all converter switching harmonics, the simulations are sufficient to identify the main relationships between grid strength, cable length, and the order of the injected harmonic. As the offshore wind demand keeps growing, this kind of design input becomes more useful, and helps the engineer make better informed decisions on grid reinforcement, cable routing, and filter design.

6.2 Key contributions

The main contributions of this thesis are:

Quantification of factor impact: The simulations show that grid strength affects the post-energization THD by an order of magnitude more than cable length does, with cable length only causing smaller shifts (1-4 percentage points) compared to grid strength (12-30 percentage points). This gives the design engineer a sense of what matters most.

Cable damping in weak grids: For weak grids, longer cables were found to reduce THD rather than increase it. This means that cable route selection should not only be based on distance and cost, but also consider power quality.

Priority orders for filter design: The harmonics observed in the results concentrate at lower orders (4th-5th), which can be used as priority targets for filter design and control system tuning.

Validation of simplified modeling: Although the model does not capture all harmonic phenomena, such as the characteristic switching harmonics from the converters, or any negative resistance behavior, it successfully identifies the dominant relationships among the parameters studied: the strong influence of grid strength on THD, the concentration of harmonic content at lower orders, and the cable length dependency that varies with grid strength. The relative importance of these grid side effects compared to converter induced harmonics is outside the scope of this model, and would require a more detailed model that captures the actual converter switching to assess.

This implies that the model is appropriate for system level harmonic studies, but detailed studying of the converter-induced harmonics would require more advanced models that

capture the power electronic switching.

6.3 Implications for the industry

For stakeholders involved with OWPPs, the results show that:

- Grid strength reinforcement gives the largest reduction in post-energization transient harmonics.
- Cable routing should consider harmonic dampening, and not solely distance.
- The harmonics captured in the aggregated model concentrate at lower orders, meaning that passive filtering tuned to these orders would address a significant share of the distortion. Filter design should in general also consider the GSC switching harmonics that were not captured by the model.
- Aggregated system level models are adequate for initial harmonic compliance studies, but detailed converter models are needed for filter sizing and analysis of switching harmonics.

For manufacturers like Hitachi Energy, the results show that:

- STATCOM control systems should prioritize compensation of lower order harmonics, which were dominant in the simulations.
- STATCOM control systems need to handle a wide range of grid strengths, since the same OWPP may see significantly different harmonic conditions as the surrounding grid changes, for example if transmission lines or generators are out of service due to maintenance or faults.

6.4 Research limitations and future studies

While the thesis achieved its primary objectives, there are some limitations:

The aggregated wind farm model is efficient for simulations, but does not capture converter switching dynamics. This means that the anticipated characteristic switching harmonics occurring around $f_{gc} \pm 2f_e$ could not be observed in this work, and determining their significance relative to grid resonances would require a more detailed model.

The fixed X/R ratio and injection of solely 5th and 9th order harmonics make up specific grid conditions. Future studies could explore other X/R ratios and injections of harmonics of other orders, such as positive sequence harmonics, in order to generalize findings.

References

[1] United Nations, "Ensure access to affordable, reliable, sustainable and modern energy." [Online]. Available: https://www.un.org/sustainabledevelopment/energy/ (visited on 2023-06-26).

[2] A. J. Kolios and U. Smolka, "Risk-based maintenance strategies for offshore wind energy assets," *2020 Annual Reliability and Maintainability Symposium (RAMS)*, 2020. [Online]. Available: https://doi.org/10.1109/RAMS48030.2020.9153642 (visited on 2023-06-25).

[3] ENECO, "Offshore wind farms shut down for first time to protect migratory birds," 2023. [Online]. Available: https://news.eneco.com/offshore-wind-farms-shut-down-for-first-time-to-protect-migratory-birds/ (visited on 2023-06-24).

[4] K.-J. Nylén, "Researcher: "marine life benefits from offshore wind power"," 2023. [Online]. Available: https://www.gu.se/en/news/researcher-marine-life-benefits-from-offshore-wind-power (visited on 2023-06-27).

[5] K. A. N. Al-Deen and H. A. Hussain, "Review of dc offshore wind farm topologies," *2021 IEEE Energy Conversion Congress and Exposition (ECCE)*, 2021. [Online]. Available: https://doi.org/10.1109/ECCE47101.2021.9595070 (visited on 2023-04-27).

[6] Elsam A/S, "Horns rev wind farm," 2002. [Online]. Available: https://web.archive.org/web/20100129161045/http://www.hornsrev.dk/Engelsk/Projektet/uk-Projektet.htm (visited on 2023-03-17).

[7] F. Blaabjerg and K. Ma, "Wind energy systems," 2017. [Online]. Available: https://ieeexplore.ieee.org/stamp/stamp.jsp?tp=&arnumber=7927779&tag=1&fbclid=IwAR0BA6kW5AokzWYN7T3RfNOmsoUIajCmhfFjsXvXcseVyskjfmbPuCst9xc (visited on 2023-02-01).

[8] Ørsted A/S, "Hornsea 2, the world's largest windfarm, enters full operation," 2002. [Online]. Available: https://orsted.com/en/media/newsroom/news/2022/08/20220831559011 (visited on 2023-03-17).

[9] J. O. Tande, O. Anaya-Lara, K. Uhlen, and K. Merz, *Offshore Wind Energy Technology*. 2018, ISBN: 9781119097792. (visited on 2023-02-12).

[10] O. Anaya-Lara, D. Campos-Gaona, E. Moreno-Goytia, and G. Adam, *Offshore Wind Energy Generation : Control, Protection, and Integration to Electrical Systems*. 2014, ISBN: 9781118701539. (visited on 2023-02-12).

[11] A. Hołdyk and Ł. H. Kocewiak, "Offshore wind power plants with 66 kv collection grids study of resonance frequencies," 2017. [Online]. Available: https://www.sintef.no/globalassets/project/eeradeepwind2017/posters/b_holdyk.pdf (visited on 2023-02-03).

[12] M.-A. Faedy and I. Scian, "Windstar – world's first large 33 and 66 kv offshore wind turbine transformer," 2018. [Online]. Available: https://search.abb.com/library/Download.aspx?DocumentID=9AKK107046A1094&LanguageCode=en&DocumentPartId=&Action=Launch (visited on 2023-02-03).

[13] L. H. Kocewiak, *Harmonics in large offshore wind farms*. 2012, ISBN: 978-87-92846-04-4. (visited on 2023-01-31).

[14] Q. Sun *et al.*, "Investigation on multiple reignitions caused by vacuum circuit breaker switching off shunt reactor considering contact travel in offshore wind farms," *IEEE Transactions on Power Delivery*, 2023. [Online]. Available: https://doi.org/10.1109/TPWRD.2023.3241407 (visited on 2023-05-28).

[15] A. Bråve and S. Särnblad, "Reactive power compensation of the electricity grid with largescale offshore wind farms in sweden," M.S. thesis, 2022. [Online]. Available: https://www.diva-portal.org/smash/get/diva2:1672800/FULLTEXT01.pdf (visited on 2023-05-20).

[16] L. Colla, F. M. Gatta, A. Geri, S. Lauria, and M. Maccioni, "Steady-state operation of very long ehv ac cable lines," *2009 IEEE Bucharest PowerTech*, 2009. [Online]. Available: https://doi.org/10.1109/PTC.2009.5282164 (visited on 2023-05-28).

[17] S. Lauria, F. M. Gatta, and L. Colla, "Shunt compensation of ehv cables and mixed overhead-cable lines," *2007 IEEE Lausanne Power Tech*, 2007. [Online]. Available: https://doi.org/10.1109/PCT.2007.4538511 (visited on 2023-05-28).

[18] M. K. Bakhshizadeh *et al.*, "Harmonic modelling, propagation and mitigation for large wind power plants connected via long hvac cables: Review and outlook of current research," *2016 IEEE International Energy Conference (ENERGYCON)*, 2016. [Online]. Available: https://ieeexplore.ieee.org/document/7513982/ (visited on 2023-02-02).

[19] R. M. Vidaurre and M. Z. Fortes, "The interaction of submarine cables and the power quality of an oil rig's electrical system," *Electrical Engineering*, 2020. [Online]. Available: https://doi.org/10.1007/s00202-020-00972-1 (visited on 2023-04-05).

[20] M. Matre, "Harmonics in photovoltaic inverters mitigation techniques," 2020. [Online]. Available: https://www.sterlingandwilsonre.com/images/knowledge-corner/pdfs/Harmonics%20in%20Photovoltaic%20Inverters%20&%20Mitigation%20Techniques.pdf (visited on 2023-05-26).

[21] N. Shah, "Harmonics in power systems causes, effects and control," 2013. [Online]. Available: https://assets.new.siemens.com/siemens/assets/api/uuid:8ab2a02e-ad94-41cb-a362-438f016aa704/drive-harmonics-in-power-systems-whitepaper.pdf (visited on 2023-05-26).

[22] F. Blaabjerg, *Control of Power Electronic Converters and Systems*. 2021, ch. Grid-following and grid-forming PV and wind turbines, ISBN: 978-0-12-819432-4. (visited on 2023-02-12).

[23] P. Roos, "A comparison of grid-forming and grid-following control of vscs," M.S. thesis, 2020. [Online]. Available: https://www.diva-portal.org/smash/get/diva2:1444307/FULLTEXT01.pdf (visited on 2023-05-20).

[24] X. Wang, M. G. Taul, H. Wu, Y. Liao, F. Blaabjerg, and L. Harnefors, "Grid-synchronization stability of converter-based resources—an overview," *2020 An-*

nual Reliability and Maintainability Symposium (RAMS), 2020. [Online]. Available: https://doi.org/10.1109/OJIA.2020.3020392 (visited on 2023-06-28).

[25] S. Zhang, S. Jiang, X. Lu, B. Ge, and F. Z. Peng, "Resonance issues and damping techniques for grid-connected inverters with long transmission cable," *IEEE Transactions on Power Electronics (Volume: 29, Issue: 1, January 2014)*, 2013. [Online]. Available: https://doi.org/10.1109/TPEL.2013.2253127 (visited on 2023-04-05).

[26] K. Hilberg, "Appendix i-g submarine export and onshore interconnection cable routes determination," 2023. [Online]. Available: https://www.boem.gov/sites/default/files/documents/renewable-energy/state-activities/Appendix%20I-G_SubmarineExportOnshoreInterconnectionCableRoutesSummary__REDACTED.pdf (visited on 2023-04-12).

[27] Ørsted A/S, "Hornsea project two offshore wind farm safety zone application," 2020. [Online]. Available: https://orstedcdn.azureedge.net/-/media/www/docs/corp/uk/hornsea-project-two/how02offex-safety-zone-application-03767092a.ashx?rev=1952f1fa61904a7eba9e30abcc5a4e28&hash=7F0225AE8BD96F602CB08A33894D620E (visited on 2023-02-21).

[28] Exponent, Inc, "Revolution wind farm offshore electric- and magnetic-field assessment," 2021. [Online]. Available: https://www.boem.gov/sites/default/files/documents/renewable-energy/state-activities/App_Q1%20RevolutionWind_Offshore_EMF_Assessment_880MW.pdf (visited on 2023-03-11).

[29] S. M.-G. M.H.J. Bollen and S. Bahramirad, "Harmonic resonances due to transmission-system cables," 2014. [Online]. Available: https://icrepq.com/icrepq'14/463.14-Bollen.pdf (visited on 2023-03-06).

[30] J. B. Glasdam, *Harmonics in Offshore Wind Power Plants Application of Power Electronic Devices in Transmission Systems*. 2015, ISBN: 978-3-319-26476-9. (visited on 2023-01-27).

[31] C. Nordling and J. Österman, *Physics Handbook for Science and Engineering*, 8:15. 2006, ISBN: 9789144044538.

[32] J. C. Del-Pino-López, P. Cruz-Romero, and L. C. Sánchez-Díaz, "Loss allocation in submarine armored three-core hvac power cables," *2020 IEEE International Conference on Environment and Electrical Engineering and 2020 IEEE Industrial and Commercial Power Systems Europe (EEEIC / ICPS Europe)*, 2020. [Online]. Available: https://doi.org/10.1109/EEEIC/ICPSEurope49358.2020.9160829 (visited on 2023-04-05).

[33] C. C. Uydur and O. Arikan, "Dielectric performance analysis of laboratory aged power cable under harmonic voltages," *Electrical Engineering*, vol. 104, pp. 4197–4212, 2022. (visited on 2023-05-25).

[34] W. Wang, X. Yan, S. Li, L. Zhang, J. Ouyang, and X. Ni, "Failure of submarine cables used in high-voltage power transmission: Characteristics, mechanisms, key issues and prospects," *IET Generation, Transmission and Distribution Volume 15, Issue9*, 2021. [Online]. Available: https://doi.org/10.1049/gtd2.12117 (visited on 2023-04-05).

[35] D. V. Hertem, O. Gomis-Bellmunt, and J. Liang, *HVDC Grids: For Offshore and Supergrid of the Future*. 2016, ch. Offshore Wind Power Plants (OWPPS), ISBN: 9781119115243. (visited on 2023-01-27).

[36] B. S. Bukh, C. L. Bak, and F. M. F. da Silva, "Analysis of harmonic propagation in power systems using standing waves," *2022 20th International Conference on Harmonics Quality of Power (ICHQP)*, 2022. [Online]. Available: https://doi.org/10.1109/ICHQP53011.2022.9808551 (visited on 2023-05-28).

[37] B. Gladstone and H. Pajooman, "Power transformer attenuates harmonics," 2004. [Online]. Available: https://www.electronicdesign.com/content/article/21187435/power-transformer-attenuates-harmonics (visited on 2023-02-21).

[38] L. Mari, "Characteristics and uses of zig-zag and wye-delta grounding transformers," 2020. [Online]. Available: https://eepower.com/technical-articles/characteristics-and-uses-zig-zag--and-wye-delta-grounding-transformers/# (visited on 2023-02-21).

[39] Å. Sjödin, "Elkvalitetsguide - för elanvändare och allmänt sakkunniga inom elområdet," 2007. [Online]. Available: https://energiforskmedia.blob.core.windows.net/media/19568/emc-elkvalitet-och-elmiljo-guide-for-elanvandare-och-allmant-sakkunniga-inom-elomradet-ny-version-januari-2007-elforskrapport-2007-40.pdf (visited on 2023-05-24).

[40] E. Csanyi, "What are triplen harmonics and where do they happen?" 2018. [Online]. Available: https://electrical-engineering-portal.com/what-are-triplen-harmonics (visited on 2023-02-21).

[41] B. Kanna and S. N. Singh, "Predictive short-term orpd in large wind farms for minimization of losses and oltc tap movements," *2016 National Power Systems Conference (NPSC)*, 2016. [Online]. Available: https://doi.org/10.1109/NPSC.2016.7858982 (visited on 2023-02-21).

[42] B. Hoseinzadeh and F. Blaabjerg, "A novel control technique for on-load tap changer to enlarge the reactive power capability of wind power plants," *IET Generation, Transmission and Distribution*, vol. 16, pp. 2928–2938, 2022. [Online]. Available: https://doi.org/10.1049/gtd2.12510 (visited on 2023-02-21).

[43] M. Christiano, "Transformer isolation," 2015. [Online]. Available: https://www.allaboutcircuits.com/technical-articles/transformer-isolation/ (visited on 2023-05-26).

[44] "Connection of wind farms to weak ac networks working group b4.62," Technical Brochure 671, 2016-12, ISBN: 978-2-85873-374-3. [Online]. Available: https://e-cigre.org/publication/671-connection-of-wind-farms-to-weak-ac-networks (visited on 2023-05-20).

[45] E. Andersson and F. Wengberg, "Utvärdering av konsekvenserna för nätanslutning av vindkraftparker i sverige vid införandet av nätkoden requirements for generators," M.S. thesis, 2015. [Online]. Available: https://www.diva-portal.org/smash/get/diva2:827469/FULLTEXT01.pdf (visited on 2023-02-06).

[46] B. Vilmann, P. J. Randewijk, H. Jóhannsson, J. Hjerrild, and A. Khalil, "Frequency and voltage compliance capabilities of grid-forming wind turbines in offshore wind farms in weak ac grids," *Electronics. 2023; 12(5):1114*, 2023. [Online]. Available: https://doi.org/10.3390/electronics12051114 (visited on 2023-05-25).

[47] P. A. Lynn, *Onshore and Offshore Wind Energy : An Introduction*. 2011, ISBN: 9781119954606. (visited on 2023-02-06).

[48] M. Mohseni and S. M. Islam, "Review of international grid codes for wind power integration: Diversity, technology and a case for global standard," *Renewable and Sustainable Energy Reviews 16 (2012) 3876–3890*, 2012. [Online]. Available: https://doi.org/10.1016/j.rser.2012.03.039 (visited on 2023-06-20).

[49] A. Anisie *et al.*, "Grid codes for renewable powered systems," 2022, ISBN: 978-92-9260-427-1. [Online]. Available: https://www.irena.org/publications/2022/Apr/Grid-codes-for-renewable-powered-systems (visited on 2023-02-08).

[50] Europeiska unionens officiella tidning, "Kommissionens förordning (eu) 2016/631 av den 14 april 2016 om fastställande av nätföreskrifter med krav för nätanslutning av generatorer," 2016. [Online]. Available: https://eur-lex.europa.eu/legal-content/SV/TXT/PDF/?uri=CELEX:32016R0631&from=PL (visited on 2023-05-24).

[51] Svenska kraftnät, "Kraftparksmodul: Bilaga 5," 2021. [Online]. Available: https://www.svk.se/siteassets/1.om-kraftsystemet/legalt-ramverk/eu-lagstiftning/anslutningskoder/bilaga-5-simulering_kraftparksmodul.pdf (visited on 2023-05-26).

[52] National Grid Electricity System Operator Limited, "The grid code," *THE GRID CODE ISSUE 6 REVISION 16*, 2023. [Online]. Available: https://eepublicdownloads.blob.core.windows.net/public-cdn-container/clean-documents/Network%20codes%20documents/Active%20Library/uk_00_FULL_GRID_CODE_I6R16.pdf (visited on 2023-06-22).

[53] Energy Networks Association, "Engineering recommendation g5," *Engineering Recommendation G5 Issue 5 2020*, 2020. [Online]. Available: https://dcode.org.uk/assets/uploads/ENA_EREC_G5_Issue_5__2020_.pdf (visited on 2023-06-19).

[54] J. Arrillaga and N. R. Watson, *Power System Harmonics, 2nd Edition*. 2003, ISBN: 9780470851296. (visited on 2023-05-20).

[55] V. Preciado, M. Madrigal, E. Muljadi, and V. Gevorgian, "Harmonics in a wind power plant," *2015 IEEE Power Energy Society General Meeting*, 2015. [Online]. Available: https://ieeexplore.ieee.org/document/7285774 (visited on 2023-03-27).

[56] J. C. Das, *Power System Harmonics and Passive Filter Designs*, 1st. John Wiley & Sons, Inc., 2015, ISBN: 9781118887059. [Online]. Available: https://doi.org/10.1002/9781118887059 (visited on 2023-06-23).

[57] J. D. Glover, M. S. Sarma, and T. J. Overbye, *POWER SYSTEM ANALYSIS AND DESIGN*, 5th. Cengage Learning, 2012, ISBN: 978-1-111-42579-1. (visited on 2023-06-21).

[58] M. H. J. Bollen, S. Cundeva, S. K. Rönnberg, M. Wahlberg, K. Yang, and L. Yao, "A wind park emitting characteristic and non-characteristic harmonics," 2010. [Online]. Available: https://doi.org/10.1109/EPEPEMC.2010.5606534 (visited on 2023-05-20).

[59] G.-L. Xie, B.-H. Zhang, Y. Li, and C.-X. Mao, "Harmonic propagation and interaction evaluation between small scale wind farms and nonlinear loads," *Energies*

2013, 6, 3297-3322, 2013. [Online]. Available: https://doi.org/10.3390/en6073297 (visited on 2023-05-20).

[60] I. Mrčela, D. Sumina, F. Sačić, and T. Bariša, "A wind turbine two level back-to-back converter power loss study," *2016 IEEE International Power Electronics and Motion Control Conference (PEMC)*, 2016. [Online]. Available: https://doi.org/10.1109/EPEPEMC.2016.7752016 (visited on 2023-05-20).

[61] S. Sang, C. Z. X. Cai, M. Molinas, J. Zhang, and F. Rao, "Control of a type-iv wind turbine with the capability of robust grid-synchronization and inertial response for weak grid stable operation," *IEEE Access (Volume: 7)*, 2019. [Online]. Available: https://doi.org/10.1109/ACCESS.2019.2914334 (visited on 2023-02-02).

[62] S. Lundberg, "Wind farm configuration and energy efficiency studies - series dc versus ac layouts," Ph.D. dissertation, 2006. [Online]. Available: https://research.chalmers.se/publication/24835 (visited on 2023-05-20).

[63] M. Bajaj and A. K. Singh, "Design and analysis of optimal passive filters for increasing the harmonic-constrained hosting capacity of inverter-based dg systems in non-sinusoidal grids," *Electr Eng 104, 1883–1907 (2022)*, 2021. [Online]. Available: https://doi.org/10.1007/s00202-021-01415-1 (visited on 2023-05-26).

[64] J. C. Das, "Passive filters - potentialities and limitations," *2016 17th International Conference on Harmonics and Quality of Power (ICHQP)*, 2004. [Online]. Available: https://doi.org/10.1109/TIA.2003.821666 (visited on 2023-05-26).

[65] L. Motta and N. Faúndes, "Active / passive harmonic filters: Applications, challenges trends," *2016 17th International Conference on Harmonics and Quality of Power (ICHQP)*, 2016. [Online]. Available: https://doi.org/10.1109/ICHQP.2016.7783319 (visited on 2023-05-26).

[66] "IEEE Recommended Practice and Requirements for Harmonic Control in Electric Power Systems," IEEE Std 519™-2014, 2014-06, ISBN: 978-0-7381-9005-1. [Online]. Available: https://doi.org/10.1109/IEEESTD.2014.6826459 (visited on 2023-05-25).

[67] Kjell Co Elektronik AB, "Växelström," 2018. [Online]. Available: https://www.kjell.com/se/kunskap/hur-funkar-det/elelektronik/starkstrom/vaxelstrom (visited on 2023-05-25).

[68] F. Ayalew, S. Hussen, and G. K. Pasam, "Reactive power compensation: A review," *International Journal of Engineering Applied Sciences and Technology*, vol. 3, no. 11, pp. 1–7, 2019. [Online]. Available: http://ijeast.com/papers/1-7,Tesma311,IJEAST.pdf (visited on 2023-05-28).

[69] F. O. Igbinovia, G. Fandi, J. Švec, Z. Müller, and J. Tlusty, "Comparative review of reactive power compensation technologies," *2015 16th International Scientific Conference on Electric Power Engineering (EPE)*, 2015. [Online]. Available: https://doi.org/10.1109/EPE.2015.7161066 (visited on 2023-05-28).

[70] F. Mays, "Negative resistance: Real or imaginary?" 2020. [Online]. Available: https://www.venableinstruments.com/blog/negative-resistance (visited on 2023-05-28).

[71] T. Messo, J. Jokipii, A. Mäkinen, and T. Suntio, "Modeling the grid synchronization induced negative-resistor-like behavior in the output impedance of a three-phase photovoltaic inverter," *2013 4th IEEE International Symposium on Power*

Electronics for Distributed Generation Systems (PEDG), 2013. [Online]. Available: https://doi.org/10.1109/PEDG.2013.6785602 (visited on 2023-05-28).

[72] L. Zhu, L. Chen, P. Hu, Y. Wu, M. Liao, and M. Xu, "Performance analysis of modeling scale on multiband oscillations in grid-connected wind farm," *Front. Energy Res., 23 May 2023 Sec. Process and Energy Systems Engineering Volume 11 - 2023*, 2023. [Online]. Available: https://doi.org/10.3389/fenrg.2023.1184119 (visited on 2023-05-28).

[73] Y. Yang, L. Yuan, Z. Qin, and H. Liu, "Wind farm resonance characteristics analysis based on harmonic impedance measurement method," *Journal of Power Electronics*, vol. 20, pp. 980–990, 2020. [Online]. Available: https://doi.org/10.1007/s43236-020-00076-w (visited on 2023-05-28).

[74] J. Kwon, X. Wang, and F. Blaabjerg, "Impedance based analysis and design of harmonic resonant controller for a wide range of grid impedance," *2014 IEEE 5th International Symposium on Power Electronics for Distributed Generation Systems (PEDG)*, 2014. [Online]. Available: https://doi.org/10.1109/PEDG.2014.6878628 (visited on 2023-05-28).

[75] ABB AB, "Xlpe submarine cable systems attachment to xlpe land cable systems - user´s guide," 2010. [Online]. Available: https://new.abb.com/docs/default-source/ewea-doc/xlpe-submarine-cable-systems-2gm5007.pdf (visited on 2023-04-27).

[76] X. Xu *et al.*, "Research on reactive power compensation system of offshore wind farm," *2019 Chinese Control And Decision Conference (CCDC)*, 2019. [Online]. Available: https://doi.org/10.1109/CCDC.2019.8833141 (visited on 2023-05-28).

[77] G. Liu, M. Fan, P. Wang, and M. Zheng, "Study on reactive power compensation strategies for long distance submarine cables considering electrothermal coordination," *Journal of Marine Science and Engineering 9, no. 1: 90*, 2021. [Online]. Available: https://doi.org/10.3390/jmse9010090 (visited on 2023-05-05).

[78] A. Fonseca, G. Salazar, F. Quilumba, and F. Pérez-Yauli, "Determination of the thevenin equivalent in power grids using real records based on short circuit power," *IET Generation, Transmission and Distribution*, vol. 15, no. 1, pp. 13–23, 2021. [Online]. Available: https://doi.org/10.1049/gtd2.12003 (visited on 2023-04-27).

[79] Siemens Energy, "The role of short circuit power for grid stability." [Online]. Available: https://www.siemens-energy.com/uk/en/energy/the-role-of-short-circuit-power-for-grid-stability.html (visited on 2023-05-27).

[80] A. V. Oppenheim and R. W. Schafer, *Discrete-Time Signal Processing*, 3rd. Pearson, 2014, ISBN: 978-1-292-02572-8. (visited on 2023-06-28).

[81] Ł. H. Kocewiak *et al.*, "Power quality improvement of wind power plants by active filters embedded in statcoms," 2016. [Online]. Available: http://lukasz.kocewiak.eu/index.php?publication=201611%20-%20Power%20Quality%20Improvement%20of%20WPPs%20by%20AFs%20Embedded%20in%20STATCOMs (visited on 2023-05-26).

DEPARTMENT OF ELECTRICAL ENGINEERING
CHALMERS UNIVERSITY OF TECHNOLOGY
Gothenburg, Sweden
chalmers.se

CHALMERS
UNIVERSITY OF TECHNOLOGY